An investigation into effects of temperature distribution on structural dynamics of bridges

A Comparative Study of Finite Element Methods and Field Data

Structural Health Monitoring

Blendi Gazidede

UNIVERSITY OF TWENTE.

An investigation into effects of temperature distribution on structural dynamics of bridges

A Comparative Study of Finite Element Methods and Field Data

by

Blendi Gazidede

in partial fulfillment of the requirements for the degree of

Bachelor of Science

in Civil Engineering

at the University of Twente,

to be defended on Tuesday June 18, 2024.

Student number:	2731681
Supervisor:	dr.ir. Roland Kromanis
Examiner:	dr.ir. Rick Hogeboom
Project duration:	April, 2024 - June, 2024
Department:	Civil Engineering
Faculty:	Engineering Technology

UNIVERSITY OF TWENTE.

Preface

This thesis culminates my three-year academic journey at the University of Twente. The research has been developed under the supervision of dr. Roland Kromanis, part of the research team in SHM for smart infrastructure. This project aims to develop the current knowledge about temperature effects in a bridge's structural dynamics by facilitating a comparison between field data and finite element methods.

I want to express my gratitude to dr. Roland Kromanis for his unwavering dedication to expanding my intellectual horizons with his consistent support in times of need. The real-world challenges require critical thinking and analytical examination - features that have been continuously highlighted in my collaboration with dr. Kromanis. His guidance has given me more than thesis support, as his way of knowledge production has made me reflect more on my aspirations as an engineer by understanding our crucial role in society.

My friends at UT have been a source of joy and motivation during times of difficulty and pressure. I want to thank all those who shared with me their experiences, from which I have been able to grow as a better friend, student, and future engineer.

Finally, I express my heartfelt gratitude to my mother and father who have supported me in every step of my life and always put their trust in me. Any achievement is meaningless to me if you are not there, thus I thank you from the bottom of my heart. This work is dedicated to my two younger brothers, Ilirian and Besjan to whom I strive to set a commendable example - not only as a student but also as a brother and as a citizen of the society.

I hope you enjoy the read!

Blendi Gazidede
Enschede, June 2024

Abstract

The aging infrastructure has accelerated the engineers' efforts to update the structural health evaluation frameworks by adapting to the ever-changing spatial and temporal parameters such as temperature distribution. Long-term monitoring studies consistently highlight the impact of temperature on bridge behavior. Solar radiation, the primary driver of temperature conditions, depends on the seasonal and diurnal sun trajectories, weather conditions, bridge positioning, and surrounding objects. The confluence of these parameters causes variations in the temperature distributions in bridges, necessitating a component-based measurement, conducted by a system of sensors attached to the deck, cables, girders, etc.

This BSc research investigates the temperature effects on the bridge dynamic response using a comparative study between field data and finite element methods (FEM). This study examines the UT Campus bridge by extracting five temperature scenarios describing distinct bridge conditions from a temperature analysis of historical data. The bridge's main dynamic parameters (natural frequencies and mode shapes) are evaluated based on the Fast Fourier Transformation (FFT) of acceleration data collected in a controlled environment experimentation.

Numerical replicas of the bridge using finite element modeling software (ANSYS) are used to approximate bridge dynamic behavior. With the objective of this research to investigate temperature-induced effects, two main modeling input parameters are determined: the bridge properties including geometry, material characteristics, boundary conditions, and the temperature distribution in the bridge. The predefined bridge material properties and geometry are refined through model updating techniques to match the bridge dynamic parameters. Meanwhile, the temperature scenarios are adopted to characterize bridge thermal conditions, with temperature as a force exerted in the elements of the FE model. The simulated frequencies from the FEM are compared to the observed frequencies from the scenario-based acceleration data via statistical and modal error indicators.

Conclusively, the FEM predicts the trend of change; a decrease in eigenfrequency as the average temperature increases, while not missing the impact of temperature variability in the structure to play a significant role. Nevertheless, it is significantly less sensitive to the rate of change compared with the observed data. Future research on transient thermal analysis alongside scenario-based controlled experimenting for the observed data can reduce the data uncertainties as well as increase the resolution of the dynamic loading interaction in bridges.

Contents

List of Figures

List of Tables

Nomenclature

Abbreviations

Abbreviation	Definition
APDL	ANSYS Parametric Design Language
FEA	Finite Element Analysis
FEM	Finite Element Method
FFT	Fast Fourier Transformation
MAC	Modal Assurance Criterion
ML	Machine Learning
PSD	Power Spectral Density
RMSE	Root Mean Square Error
SHM	Structural Health Monitoring

Symbols

Symbol	Definition	Unit
f_n	Natural frequency	[Hz]
K_n	Effective stiffness coefficient	[-]
E	Young's modulus	[N/m^2]
I	Moment of inertia	[m^4]
w	Density of the material	[kg/m^3]
g	Gravitational acceleration	[m/s^2]
L	Length of the specimen	[m]
ϕ_o	Mode shape vector (observed)	[-]
ϕ_e	Mode shape vector (expected)	[-]

1

Introduction

Bridges are essential parts of the infrastructure; being pivotal for the transportation of people and improving inter-regional accessibility, contributing to the economy by facilitating trade and commerce, and overall being a symbol of development and quality of life. Their serviceability is crucial for the progress of the mentioned societal dynamics, therefore bridges as many other civil engineering structures are designed for a relatively long lifespan with most of the bridges in the Netherlands exceeding 50 years in functionality (Rijkswaterstaat, 2022). Throughout the years, the environmental impact, notably the temperature distribution alongside the traffic loading has affected the structural integrity of these bridges, some being extensively deteriorated and the remaining raising concerns for damage (Sohn (2006); Figueiredo et al. (2024)). This natural degradation of structures under variable conditions has necessitated the need for Structural Health Monitoring (SHM) to assess the reliability of using these structures. Nowadays, bridges are continuously monitored structures compared with other infrastructure components. These inspections, mostly conducted as visual monitoring are traditionally focused on fatigue detection via comparison with standardized qualities of the bridge elements set by international guidelines on material properties; which include cracks, corrosion, deformation, vegetation, etc. Nevertheless, such inspections are based on empirical quantification of damage and are inherently prone to human error while being unable to address the degree to which temperature affects structural behavior.

The increased interest in the investigation of the environmental impact of bridge response has catalyzed shifts in the way structural health monitoring is conceptualized. In the early 1960s when SHM was presented as a new framework to verify the structural conditions of a bridge based on modal analysis of sensor-collected data, there was no novelty in the introduced practice on how to account for damage and how to understand the material-to-environment relationship. With the development of technology, data analyses become prominent in engineering, thus highlighting the importance of the data-gathering function of the existing SHM systems (Koo et al. (2012); Tadeu et al. (2022); Glashier et al. (2024)). The data-driven approaches provide valuable insights into the dynamics of the bridge, however, localization of damage and impacting variables such as temperature, wind, and humidity are assessed qualitatively due to the lack of controlled experimenting of isolated inputs.

SHM techniques have evolved rapidly in the last years, since the introduction of finite element methods (FEM) in civil engineering. This numerical technique built upon the finite fragmentation of structures into simpler units governed by systems of equations describing the laws of physics and reacting phenomena, allowed engineers and researchers to isolate and adjust dimensions and material properties of structures while controlling the input conditions such as temperature distribution and humidity. This method exhausted the continuous struggle of testing in bridges, by inducing extreme scenario conditions, normally unachievable in real-life settings (Rao, 2017). Furthermore, it has spurred a deeper understanding of bridge behavior reflected the dynamic parameters such as natural frequency and mode shapes.

This research aims to contribute to the existing knowledge in SHM by establishing a comparative study of long-term measured data and finite element modeling. Specifically, the study investigates the impact of temperature distribution on the bridge dynamic response. A case study is presented to exemplify a practical application of this method. Initially, collected data from a system of sensors is analyzed, and filtered on a frequency domain. Subsequently, the bridge model is built in FEM software (ANSYS) and is updated based on a reference scenario of established knowledge about dynamic parameters and uniform temperature distribution. The outputs of the model, consisting of dynamic properties such as natural frequencies are compared with the observed frequencies to investigate the feasibility of FE modeling in predicting bridge response under variable temperature conditions.

1.1. Long-term bridge monitoring

The baseline for this research is to understand the bridge behavior under temperature distribution using a sensor-based monitoring system. The long-term monitoring system is the primary mechanism to collect data that describe the dynamics of a bridge and the surrounding parameters, enabling a possibility for a simultaneous 'system snapshot' that can help engineers assess the relationship between observable and non-observable factors. For data acquisition, the utilized sensors are accelerometers, strain gauges, and temperature sensors.

Accelerometers are the vibration recorders of the bridge. If the bridge is excited causing a sudden or continuous shift from the state of equilibrium, vibration sensors record the displacement of the internal spring system by converting it to an electrical signal that records the acceleration relative to the ignited axis. While accelerometers make use of spring system sensitivity, strain gauges measure the amount of strain caused by a force-based deformation such as tension, compression, bending, or torsion based on the electrical resistance of the material. Apart from the direct bridge response measurements, the dynamics of the bridge account for the temperature conditions of these measurements. Temperature sensors or thermocouples measure the bridge's thermal environment by approximating temperature as a voltage difference between two distinct metal wires. These sensors are attached to bridge components to measure their temperature. Nevertheless, data acquisition requires thorough implementation techniques and a management plan to accurately monitor a whole system with various confluent parameters.

Sensors require strategic location planning dense spatial scattering all over the bridge (Steenackers and Guillaume, 2005). Distance between sensors is determined by bridge design, geometry, and research purpose. The position of temperature sensors is critical due to their sensitivity to solar exposure variations and the material it is attached to (Alampalli (1998); Cross et al. (2013)). These measurements require an incremental basis of repetition and storage; carried on an hourly basis for temperatures and on minute-based systems for accelerations in high-resolution systems. This necessitates bridge monitoring to be a continuous process that requires a long-term practice of management and inspection of sensors' serviceability.

The spatial and temporal characterization of bridge response derived from dissimilar sensor systems requires data synchronization to ensure correct correlation between measured indices. Subsequently, measured data are stored in accessible hard drives to be used for further analysis. A detailed analysis of the collected data is impractical due to the sheer size of the data; hence, numerical replicas of bridges are nowadays increasingly favored over data-driven models for the time efficiency and the ability to explore features impossible to be evident in the empirical models. However, any numerical model is an approximation of reality, thus hybrid approaches of comparative studies between simulations and observed data can effectively balance the strengths and limitations of the long-term structural health monitoring systems.

1.2. Research aim and objectives

This thesis investigates the effectiveness of the finite element method in estimating the temperature distribution effects in the structural behavior of the UT Campus bridge located in Enschede, the Netherlands, by conducting a comparison of simulated dynamic response with field data obtained from a continuous structural health monitoring system.

The rapid change in environmental conditions has affected the structural conditions of bridges, thus making their health assessment a perplexing work. Among the confluent factors affecting bridge structural integrity, the temperature distribution is a critical parameter. However, the existing engineering guidelines lack a deep understanding of the thermal effects on the bridge response, while data interpretation from structural health monitoring systems requires additional analytical processing, thus increasing uncertainty about data usability for impact assessment. The motivation behind assessing the effectiveness of FE simulations underpins the feasible understanding of the dynamic behavior of the bridge elements under different temperature conditions; by verifying the extent to which FE models can predict real-life structural behavior quantitatively. The model effectiveness is assessed based on the accuracy of the model to fit the real-life dynamics of the bridge, measured in terms of model error. To support these conclusions, certain research objectives are formulated:

- To analyze field data measured from the structural health monitoring system installed on the bridge, composed of distributed temperature sensors and accelerometers.
- To determine the bridge's main dynamic parameters such as natural frequencies and mode shapes alongside different temperature scenarios.
- To utilize FE simulations by designing a steel girder bridge based on its geometry, material properties, and boundary conditions.
- To update the FE model relative to established knowledge about the bridge's main dynamic parameters obtained from a controlled data acquisition campaign.
- To compare observed and simulated results via statistical and modal error indicators.
- To assess the discrepancies between observed and simulated data, by identifying possible sources of errors and by highlighting limitations of FE modeling in aiding engineers to evaluate bridge performance under variable conditions.

1.3. Scope of the study

The scope of this thesis proposal comprises an investigation into structural health monitoring practices, specifically data collection and interpretation as well as FE modeling in capturing temperature-induced effects regarding modal parameters. The investigation of the literature is presented in Chapter 2. It is elaborated in four sections, regarding structural health monitoring, structural dynamics, temperature effects on the dynamic response of bridges, and FE modeling and simulations. A three-step methodology is explained in Chapter 3, uncovering the mechanism to sufficiently extract, model, and interpret real-life phenomena features from the bridge behavior. Chapter 4 presents the study case, for which the methodology is applied. It explains the context for the temperature contributions in Section 4.1 and the relevance of the output from the data interpretation of accelerations in Section 4.2. Section 4.3 introduces the numerical representation of the UT Campus bridge alongside the model updating mechanism and temperature distribution model that implements the results from temperature analysis. Finally, the last chapters discuss the results in Chapter 5 and limitations of the research in Section 5.4, focusing on epistemological deficiency as well as empirical and modeling uncertainties.

2

Literature review

For a better understanding of the knowledge development regarding the key underlying concepts and objectives of this research, the literature is reviewed to establish key concepts and a framework for this study to further develop existing knowledge and address possible recommendations encountered from the studies in the past. This chapter initially introduces Structural Health Monitoring in Section 2.1, followed by a brief explanation of Structural Dynamics in Section 2.2, thus providing a technical domain settling for the subsequent chapters. Finally, literature concerned with temperature distribution effects on bridge dynamics and FE modeling are summarized in Section 2.3 and Section 2.4 respectively.

2.1. Structural health monitoring

Structural health monitoring (SHM) on its primary premise refers to a system utilized to monitor the behavior of a bridge under traffic load and environmental impact. At its core, it is a data-gathering system developed to record data regarding bridge response to excitation. These data are collected, filtered, processed, and analyzed by structural engineers to verify the structural integrity of infrastructure components, mostly bridges to assess the degree of safety and level of serviceability (Borah et al., 2021). Its importance is explicated by the contribution to a much more complex interface of systems and its relevance to the economy and society transcends the engineering realm, thereby developing methods to increase structural condition awareness is a cornerstone for most of the studies conducted in the SHM domain.

Defining a universal SHM framework has been a difficult task for studies in the past, because of environmental and operational variations in structures as highlighted by Sohn (2006). Understanding the measured data and isolating the effects of individual factors like temperature, and traffic have required perplexing analysis according to Koo et al. (2012). Not only data collection and analysis is challenging but even if achieved with strict rigor, means of validation with models such as FE simulations are strenuous for the updating of the condition parameters (Westgate and Brownjohn, 2011). However, some converging attempts to establish an effective paradigm to fit different contextual conditions are presented by Sohn (2006), Malekloo et al. (2021), and Figueiredo and Brownjohn (2022), with the latter one chosen to proceed in this research methodology. According to Figueiredo and Brownjohn (2022), SHM can be described as a four-stage process: (i) operational evaluation, (ii) data acquisition (iii) feature extraction and generation, and (iv) statistical modeling for feature classification. There are no defined boundaries between the stages, therefore overlapping is possible, sometimes necessary.

Operational evaluation In this stage, the motivation of the assessment and context-settling parameters of the study case are defined. It also involves answering essential questions related to the implementation of the SHM system, such as safety justifications, risk-to-damage analysis the structure, cost, duration, etc. This phase is highly sensitive to the case study and legislative regulations sectioned in engineering codes such as Eurocode and National Annex.

Data acquisition The most common data acquisition practice in bridge monitoring is vibration-based structural health monitoring. This system is composed of sensors, mainly active or passive, depending on the purpose of the monitoring process and the type of data necessary for the engineers to analyze. In the case of active sensors, they artificially excite the structure via signals to record their response, while passive sensors function as 'recorders' of the bridge's natural behavior (Cai et al., 2012). Despite the active sensors being more precise in diagnosing possible damage in a structure, the latter sensors are preferred over active sensors due to their cost-efficiency and resolution of environmental variability. Sensor types differ by nature depending on the parameters assigned to be measured, varying from acceleration, strain, temperature, etc. Other important features that influence the quality of the measured data are the sensor layout and placement in the structures alongside the density of sensors utilized.

Feature extraction and generation Feature extraction relates to a preliminary data analysis that begins with data filtering and refining, conducted manually or automatically by Machine Learning (ML) algorithms such as Artificial Neural Networks and Multilinear Principal Component Analysis (Glashier et al., 2024). This analysis aims to extract the system's responses to natural excitation in terms of damage-sensitive patterns based on model-driven or data-driven approaches. The model-driven approach emphasizes the physical understanding of the structure via numerical models to predict the bridge behavior under variable internal (inherent damage) and external (environmental and traffic) conditions. On the other hand, data-driven approaches rely on data interpretation only, thus there is limited knowledge about the structures and it relies on ML algorithms and boundary conditions set in the operational evaluation stage.

Statistical modeling for feature classification The biggest workload of data analysis occurs in this stage. It leads to an inference of the data-driven approach, by detecting any anomaly exceeding the safety boundaries set earlier on. In the model-driven approach, any sensitive change in the input features is referenced as casually related to potential damage.

Structural health monitoring reliance on data monitoring and acquisition has proven to be successful in assessing structural integrity, but its application is occasionally obstructed as a result of the reactive attitude of these systems. These are not any different from the traditional visual inspection which relies on information on the presence of damage. Therefore, resilient health monitoring has to be supported with proactive measures of damage detection, and that includes the integration of model and data into hybrid approaches, calibration, and validation of these models with continuously refreshed data and machine learning techniques assisted by artificial intelligence (Figueiredo and Brownjohn, 2022).

2.2. Structural dynamics

Structural dynamics is a branch of structural engineering focused on analyzing the behavior of structures under time-varying conditions. It studies the behavior of a structure by identifying dynamic properties such as natural frequencies, mode shapes, and damping ratios. These parameters are unique for any structure, thus any variance in their magnitude represents a specific response of the bridge to any internal and external change resulting in an overview of bridge performance. International engineering guidelines delineate the norms and conditions of the bridge depending on the magnitude of these parameters. Non-stationary ambient excitation sources such as wind, traffic, waves, etc. impact structural dynamic parameters by causing fluctuations in the collected data(Cornwell et al. (1999); H. Li et al. (2009); Cross et al. (2013)). Therefore simplistic data analysis that neglects the relative contribution of environmental variability can lead to inaccurate damage detection and erroneous decision-making (Steenackers and Guillaume, 2005).

Addressing these knowledge gaps, Farrar et al. (1994) performed a vibration test and consequently a vibration analysis in a concrete bridge to investigate the usability of modal parameters in determining damage. This vibration-based monitoring consists of vibration testing and analysis, commonly referred to as modal analysis, and is widely used in SHM studies such as the Z-24 bridge (Alampalli, 2000), the Ting Kau bridge (Ni et al., 2008), the Tamar bridge (Cross et al., 2013) to provide insight into the structural behavior of deteriorating infrastructure.

Natural frequencies and mode shapes The components of a bridge tend to deflect, varying on the stiffness and mass distribution of the material. Any stimuli inflicted on these components disturb the balance of the bridge, resulting in a change in the state of equilibrium. These changes in equilibrium are the sum of simultaneous vibration patterns, which if considered spatially over the span of the bridge, are called the mode shapes. The vibration pattern is described as the eigenfrequency or natural frequency of a bridge. Eigenfrequency describes the rate at which a structure or component oscillates, measured in Hertz (Hz). In ideal conditions, the natural frequency f_n can be calculated using the following formula:

$$f_n = \frac{K_n}{2\pi}\sqrt{\frac{EIg}{wL^4}} \qquad \text{(Eq. 2.1)}$$

where K_n is the effective stiffness coefficient for the n-th mode, E is the Young's modulus, I is the moment of inertia, w is the density of the material, g is the gravitational acceleration and L is the component's length. Under variable conditions, the predicted values from the theoretical natural frequency and the measured natural frequency do not comply. This is mainly related to the change in the stiffness of the component, where any sign of damage or impact from environmental conditions such as temperatures will cause a reduction of the stiffness, resulting in the observed eigenvalues being lower than predicted ones. Analyzing only natural frequencies does not provide details for which of the aforementioned criteria is the root cause of the behavior anomaly, thus the mode shapes are required to understand spatial deformations of the components relative to changes in natural frequencies.

2.3. Temperature effects on bridge dynamics

In the SHM context, bridges are frequently monitored to verify their structural integrity, and serviceability over time. While traditional methods such as visual inspection are commonly used to detect visible damage or deterioration, they may not provide comprehensive insights into the effects of temperature on bridge conditions. Therefore, the structural health monitoring systems are used to collect sufficient data about the dynamic response of the bridge, in terms of natural frequency and mode shapes aggregated with temperature distribution to understand the impact of the diurnal or seasonal change in these dynamic parameters. Early studies investigating the material properties (mainly part of the science of material studies) such as Rishin et al. (1973) concluded that an increase in temperature causes a decrease in the Young's modulus E of a material due to thermal expansion. Consequently, according to Equation 2.1, the results implied that the natural frequency will decrease as the temperatures increase. Prior studies in SHM tried to analyze the environmental impact on bridge behavior with Cornwell et al. (1999) conducting a modal analysis of the Alamosa Canyon bridge during daily temperature cycles. This study highlights the influence of temperature on the dynamic properties of bridges and was in the continuous support of experimental findings of material of science papers (Rishin et al., 1973) and previously conducted research on the dynamic characterization of bridges (Moorty and Roeder (1992); Farrar et al. (1994)).

Peeters and De Roeck (2000) uncovered the limitations of experimental-based investigation on the temperature effect on bridges due to the non-linear relationship of temperature and natural frequencies based on a year-long monitoring of data in Z-24 bridge. The study concluded that there is a linear relation for the temperatures above freezing point ($0\,^{\circ}\mathrm{C}$), unlike the non-linear relationship of the natural frequencies depending on the material of the component. These findings were justified by an earlier study of Alampalli (1998) which supported the reasons behind this non-linearity depending on the type of support, the presence of asphalt, exposure to solar radiation, size of the bridge, etc; later revised in Tamar bridge (Cross et al., 2013).

However, the temperature distribution becomes more complex due to seasonal changes. In the winter, the diurnal change does not affect the natural frequencies, compared to the same hourly fluctuations in temperatures in the summer. This correlates to the more uniform temperature distribution in the cold seasons compared to the variations in the spring and summer months. Laory et al. (2012) highlighted that the diurnal changes have a more significant effect in summer compared to winter. This study revealed the necessity for long-term data monitoring to reduce uncertainty about the dynamic variation of modal parameters. Recent studies managed to collect long-term data on modal parameters and temperature distributions in bridges. The case of the long-term monitoring of the Tamar bridge presented by Cross et al. (2013) revealed temperature was found to have a seasonal impact rather than daily in terms of relative change in natural frequencies depending on the uniformity of thermal strain.

Although the temperature effect was evident in most SHM studies, its quantification is crucial for effective damage detection. Understanding damage patterns necessitated regression analysis on collected data to dive into the sole effect of temperature apart from other variable conditions. Xia et al. (2006) developed a linear regression analysis to establish relationships between the measured frequencies on a reinforced concrete slab under temperature changes. The results revealed a strong negative correlation between frequency and temperature in four mode shapes, with the first two modal frequencies decreasing by 0.23% when the temperature is increased by one degree. These findings tangentially spurred a continuous strive for quantifying the impact of the temperature variation such as the case of the Tianjin Yonghe Bridge which was used as a case study in H. Li et al. (2009). This paper connected ANN, MPCA, NLPCA, and IRB analysis to quantify the change of natural frequencies at a magnitude of 1.470% to 3.155% as the temperature varied from $-11.5\,^{\circ}\mathrm{C}$ to $3.71\,^{\circ}\mathrm{C}$. Similar studies on cable-stayed bridges, footbridges, and concrete bridges are presented by Catbas et al. (2008), Kromanis et al. (2015), Tadeu et al. (2022) highlight the importance of temperature-induced stresses on bridge dynamic parameters, relative to the traffic loads.

2.4. Finite element methods

Finite element method is a numerical technique based on the fragmentation of structure or 'subject domain' into smaller and simpler units. This unit is governed by the differential equations and boundary conditions set by the field of application (e.g. fluid dynamics, structural analysis, heat distribution, soil mechanics). These units are connected via a set of nodes, constituting a mesh model or a representative of a real-life environment dictated by the mathematical model built upon. In the context of SHM, the FE modeling assists in a parametric study to investigate the influence of specific conditions, impossible to happen or improbable to be measured, in real-life structures. The primary application of FE modeling pertains to stimulating damage scenarios to verify bridge response compared with measured data. Particularly, they are employed to address thermal effects by varying temperature input to estimate the relative contribution to dynamic properties of the bridge such as natural frequencies and mode shapes (L. Zhou et al. (2015); Liu and Zhang (2017)).

Creating a numerical replica of a bridge in FEM, requires two main considerations: the bridge characteristics such as geometry and material composition, and the boundary conditions. The bridge characteristics related to the types of the bridge pose increased uncertainty in temperature-induced data depending on the number of the components, such as the case of a long-span cable-stayed bridge (Y. Zhou and Sun, 2019). On the other hand, material property estimation is bounded by our theoretical understanding of the structure and is quantified by deterministic values for Young's modulus, Poisson's ratio, and thermal expansion coefficients. These values are attributed to an ideal bridge condition, assuming uniform structural integrity, thereby posing a limitation of the analysis application. The second input, referred to as boundary conditions, is a set of limitations in terms of mathematical restrictions. These conditions define the integration of the system with internal and external forces. The internal forces are explicitly related to support reaction impact on the deformation patterns, while the external forces relate the FE model to variable input such as traffic loading or temperature distribution.

In the case of temperature impact analysis, the literature provides two possible analysis options. One method is to conduct a thermal analysis of the bridge. This analysis comprises a theoretical application of heat-transfer analysis and thermal boundary conditions in the case of a bridge environment, accounting for various meteorological conditions. Important remarks of this method are the efficiency in predicting temperature distribution which concurs with measured data (L. Zhou et al., 2015). Despite temperature distribution not being isolated from concurring with other environmental variables, there is another method that can account for specific temperature distributions, and that is temperature profiling via model updating. Model-updating techniques are applied in data-driven analysis of the bridge behavior (Cross et al. (2013); Kromanis et al. (2015); Mariani et al. (2024)) to link deformation with temperature variation. Model updating is conducted to evaluate bridge conditions, or make retrofitting schemes by systematically varying the bridge's geometrical and material properties to match observed data results (Kangas et al. (2003); Zhu et al. (2015)). For damage assessment dependent on temperature variability and traffic loading, specific temperature distributions convey complex patterns, thereby scenario-testing based on collected data can be used as part of model updating (Marchenko et al., 2024).

Westgate and Brownjohn (2011) presented an FE model of the Tamar bridge as a research tool to verify the impact of variable environmental conditions. This research concluded that adjusting the stiffness of the structure, thus virtually damaging the bridge by reducing Young's modulus takes increasing precedence over the modal properties on the later frequencies of the bridge. Nevertheless, FE modeling has its limitations where sources of error may derive from the mathematical model of the structure assuming isotropy and linear-elastic behavior, the quality of which is constrained by mesh size and computational power. Nonetheless, FEM is an approximation of reality, thus it is bound by human knowledge and computational power, as highlighted by Figueiredo and Brownjohn (2022).

2.5. Conclusions

The literature review provides foundations for understanding the key concepts and objectives of the research. SHM is introduced as a safety-assessing system for monitoring the behavior of bridges under variable loading and environmental conditions. The integration of sensors in the monitoring systems has enhanced the capability to precisely characterize the bridge dynamic response both spatially by localizing feature deviation and quantitatively by assessing the damage. The reviewed studies propose research methods that contribute to knowledge production and development of current SHM practices. Nevertheless, these studies encounter knowledge gaps, explicitly acting as boundary conditions for the reliability of the studies. The following conclusions are highlighted consistently:

1. The interchangeability of environmental conditions coupled with the uncertainty of data acquisition and extraction campaigns has posed a challenge in establishing a universal SHM framework, despite the efforts of several studies such as Sohn (2006), Malekloo et al. (2021), and Figueiredo and Brownjohn (2022).
2. The sensitivity of bridge dynamics requires long-term monitoring and temperature isolation both numerically and methodologically to verify the extent to which temperature influences the bridge dynamics spatially and temporally (Cornwell et al. (1999); Peeters and De Roeck (2000); Catbas et al. (2008); Laory et al. (2012)). Therefore, understanding the temperature effects on bridge dynamics requires hybrid approaches of observed and simulated data with perpetual cross-validation.
3. The deficiency of modeling techniques for the temperature distribution relative to the real-life measurements necessitates improvements in the model updating techniques of the FE models, specifically for the non-linear scenarios (Westgate and Brownjohn (2011); L. Zhou et al. (2015); Liu and Zhang (2017)) such as temperature distributions.

In conclusion, this chapter summarizes the main findings of the literature review conducted in support of the research objectives. These studies' limitations provide future research direction in quantifying temperature effects on dynamic parameters through advanced regression analysis or numerical techniques. The latter serves as the initiator of the research methods, for the FEM techniques being cost-effective and resilient to the environment, necessary to simulate complex temperature scenarios and assess their impact on bridge structural dynamics.

3

Methodology

A framework to investigate the impact of temperature distribution in bridge dynamic response developed by integrating long-term bridge monitoring studies (Cross et al. (2013); Kromanis et al. (2015)) and FEM of bridge behavior under variable environmental conditions (Westgate and Brownjohn (2011); Marchenko et al. (2024)). A three-step methodology, as presented in Figure 3.1, is devised to conduct this research. Initially, an operating SHM system that collects acceleration and temperature records of the environmental conditions is utilized as the main source of information for the study case. The continuously collected data is stored in a time-series database. The temperature historical dataset is analyzed where five scenarios are selected, yielding a range of conditions the bridge experiences annually. A heel-drop experiment is conducted in the bridge, to determine the bridge's natural frequencies under controlled conditions. These values are used as a reference for the comparative study further on. The second phase entails an FE model set-up with the bridge's dimensional and material characteristics and temperature distribution. A FEM software (ANSYS) is employed to run a finite element analysis (FEA) predicting the bridge behavior as opposed to real observations from the study case. The model is iteratively updated with reference to the controlled environment results to actualize real bridge behavior so it mimics real-life dynamics. Finally, a comparison between observed and simulated data is conducted through error estimation and mode assurance criterion (MAC). The detailed explanation of these three phases is explained in the next chapters grounded on the reviewed methodologies in the literature.

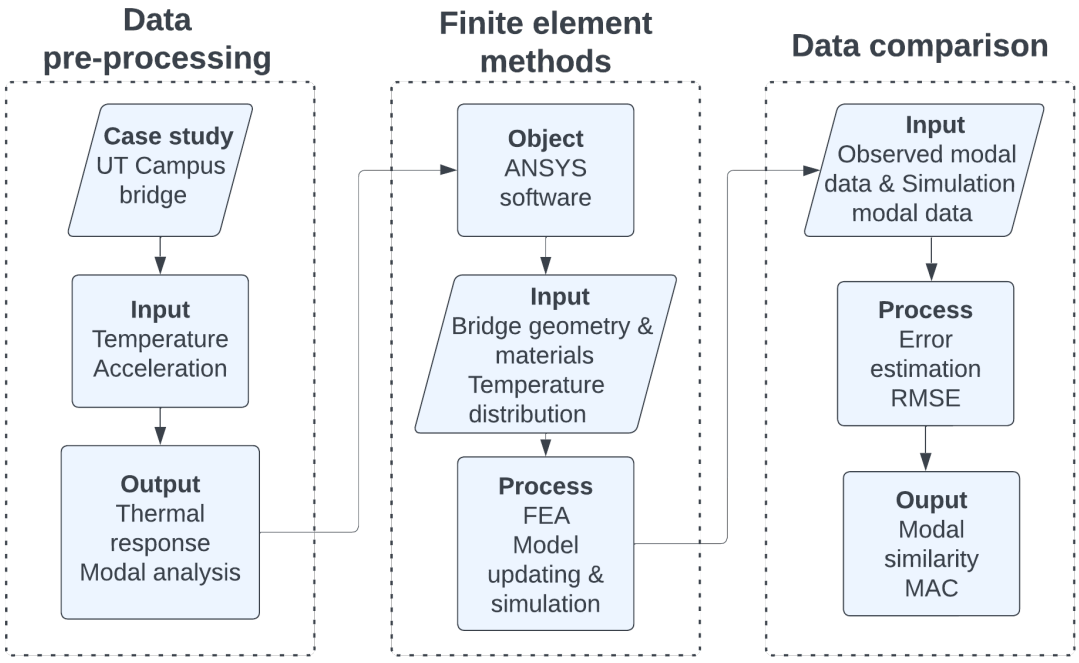

Figure 3.1: The methodological workflow of the research.

3.1. Data pre-processing

This section outlines a methodological procedure for temperature data analysis and acceleration data pre-processing. The temperature is retrieved from the historical database, while the acceleration data comprises two types: the controlled environment acceleration data used in this phase to determine the modal parameters for a reference scenario, and the uncontrolled environment acceleration data, which coincides with temperature measurements to describe bridge behavior under temperature distribution effect. The latter dataset is analyzed and compared in the last stage of this study. Additional data regarding humidity or wind speed are neglected for being outside the scope of this study.

3.1.1. Temperature data

The variation of temperature is important to isolate the thermal response and relate its effects on the bridge to the dynamic parameters. High variability in the temperature distribution causes different contractions and expansion patterns in the bridge, resulting in different stiffness-to-mass ratios for the same bridge component. This nonlinear deformation for a unit length of component i.e. the girders affects the extent to which the bridge can oscillate on its natural frequency, with the higher deformation expected to reduce the frequency measurement as discussed in the literature review, Section 2.3. An illustration of the selection criteria is displayed in Figure 3.2, representing the daily average temperature measurement of all sensors alongside the standard deviation indicated by the error bars.

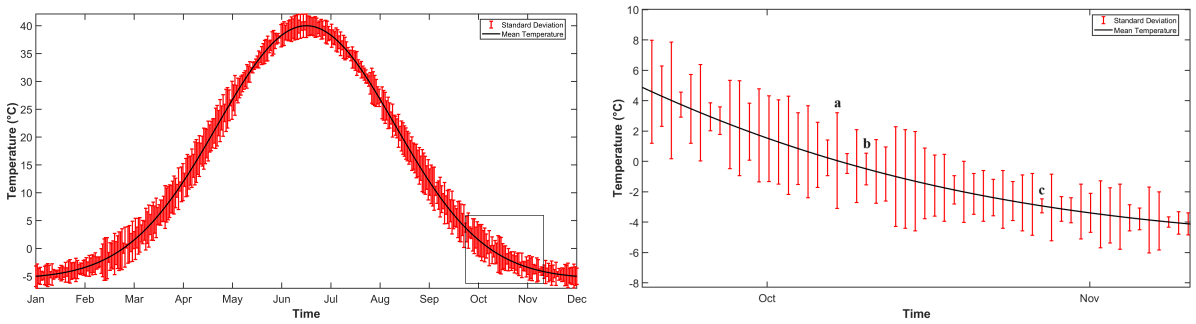

Figure 3.2: Average annual temperature distribution (left); Zoomed window for one-month duration (right).

The historical sensor measurements are analyzed to identify five distinct scenarios encompassing a wide range of diurnal and seasonal conditions. Two selection criteria are applied to categorize the magnitude of the variability; the amplitude of variation and the average and standard deviation of all measurements. These indicators quantify the change between the maximal and minimal measurement, thereby revealing the days with the highest variability indicated by the error bar (a) in Figure 3.2. Concurrently, the average and standard deviation are used to determine extremely hot scenarios for the highest average temperatures in the summer middays and extremely cold scenarios for the lowest temperatures in winter sunrise. Intermediate scenarios representing cloudy and rainy days are selected for both hot and cold seasons (error bar (b)). The solar radiation is scattered evenly in the environment, causing less variance in the temperature measurements. Finally, a low amplitude and low standard deviation (error bar (c) in Figure 3.2) for the measurements signifying a uniform temperature distribution across the structure is selected for the reference scenario. The average temperature of this scenario is consistent with the controlled experiment average temperature to ensure a basis of comparison between observed and simulated data in Chapter 5.

3.1.2. Acceleration data

The measured acceleration data coinciding with the temperature measurement can reveal a correlation between parameters, but the insufficient understanding of the loads exciting the bridge impedes the precise evaluation of the bridge's natural vibration. Consequently, a controlled experiment is conducted under constant verifiable environmental parameters such as temperature, wind, and humidity - with the bridge devoid of cyclists and pedestrians traffic. A constant point force is exerted by an individual at different locations of the bridge. The bridge response is captured via a deployed system of wireless sensors.

The eigenfrequencies or natural frequencies can be estimated using Fast Fourier Transformation (FFT), illustrated in Figure 3.3. FFT is a mathematical algorithm that computes the frequency of a signal by decomposing the relative magnitudes of the various sinusoidal signals (Rogers et al., 1997). The FFT applies for the whole signal simultaneously but loses the temporal information of the signal. The natural frequencies are selected using the peak-picking method. The frequencies with the higher amplitudes represented as spikes in the FFT graphs, denote the dominant frequencies or the natural frequencies of the bridge. Peak selection requires a thorough consideration to differentiate natural frequencies from resonant ones, with the latter characterized by sharp, prominent follow-up peaks. For the controlled environment, acceleration pre-processing is not conditioned by unknown parameters, therefore the presence of resonant frequencies is limited, making the interpretation of results straightforward.

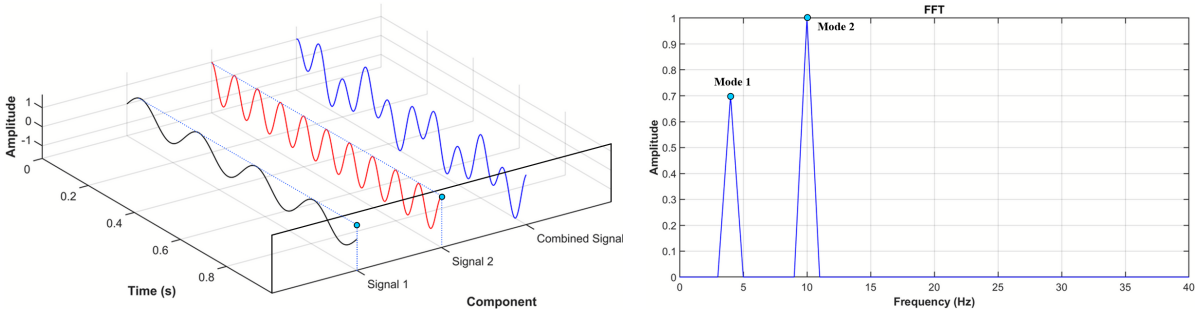

Figure 3.3: Wave signal decomposition (left); Fast Fourier Transformation for frequency estimation (right).

The mode shapes are defined by the spatial distribution of the amplitudes of the natural frequencies of a bridge. The eigenfrequencies picked in the FFT plot from Figure 3.3 for several measurements across a structure will reveal the corresponding vibration pattern such as the first vertical and first torsional mode shapes in Figure 3.4. While the frequency-amplitude plots reveal the magnitude of deformation or acceleration of a certain frequency, the phase spectrum analysis provides information about the location of a point or node in time relative to a reference frequency. It refers to the angle component describing the displacement of the sinusoidal wave relative to a reference point and is evaluated by considering the imaginary number of each frequency value calculated by the FFT. This is applied in a Matlab code, which uses the eigenfrequencies as the reference points to determine the direction of the deflection to be either positive or negative.

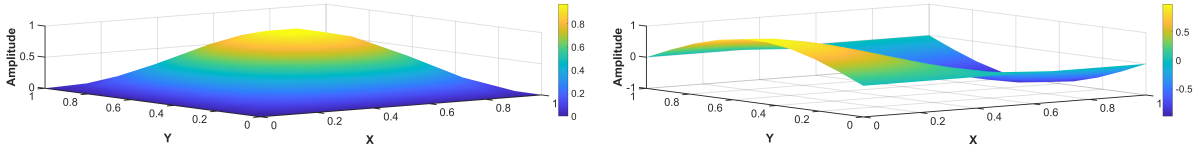

Figure 3.4: Mode shapes from the peak-picking method of the first eigenfrequency (left) and the second eigenfrequency (right).

Uncontrolled environment measurements referred to as scenario-based acceleration data present higher uncertainty. The main criteria to correlate the impact of temperature variation investigated in the previous section is by selecting bridge response concurrent with or within a time range from the time of temperature measurement. If the same time is not possible due to the desynchronization of the two measuring systems or because of disturbance due to abnormal accelerations, then the range of 15 minutes is considered a representative of the bridge response due to the given temperature configuration. This presumes the relatively slow heat transfer for a limited time window, reflected by the similar values of the temperature standard deviation.

The second criterion is the scenario selection. The sensors collect acceleration data from all kinds of excitation such as walking pedestrians, cyclists, wind, etc. thus consisting of uncontrolled testing conditions. Correlating temperature to any change of frequency pattern would require considering the relative impact of these other factors which are unknown and cannot be quantified. Therefore the selection criteria are narrowed to cyclists-induced accelerations, thereby neglecting any pedestrian measurement. The higher speeds reflected by smaller time measurements are less likely to cause resonant effects compared to the walking-induced frequencies which may coincide with bridge natural frequencies and alter the bridge response.

3.2. Finite element methods

The FEM is a numerical technique designed to systematically solve complex problems by fragmentation of the subject matter. The subject matter ranges from solid to fluid objects and is dependent on the scope of the study. The most common procedure for developing a FEM requires the geometry design with context-dependent reference elements, the material characterization with properties describing its behavior under input forces, and the assignment of the boundary conditions to describe the constraints of a subject matter's behavior.

In bridge modeling, the division of the structure into finite elements, also known as discretization, represents the building block of the entire structure. These fundamental units are interconnected via nodes, which are specific points in the structure that describe the relations between elements in terms of translation and rotation. Node allocation can be in the boundaries between elements or within an element, depending on the nature of the problem. The shape of the elements depends on the dimensionality of the problem, where the one-dimensional problems require line elements, increasing to triangular and quadrilateral shapes for two-dimensional problems (Figure 3.5) up to tetrahedral or hexahedral for three-dimensional domains (Rao, 2017). The nodal network is the functional unit that connects the physical condition assigned to the elements with the governing equation of the modeling continuum.

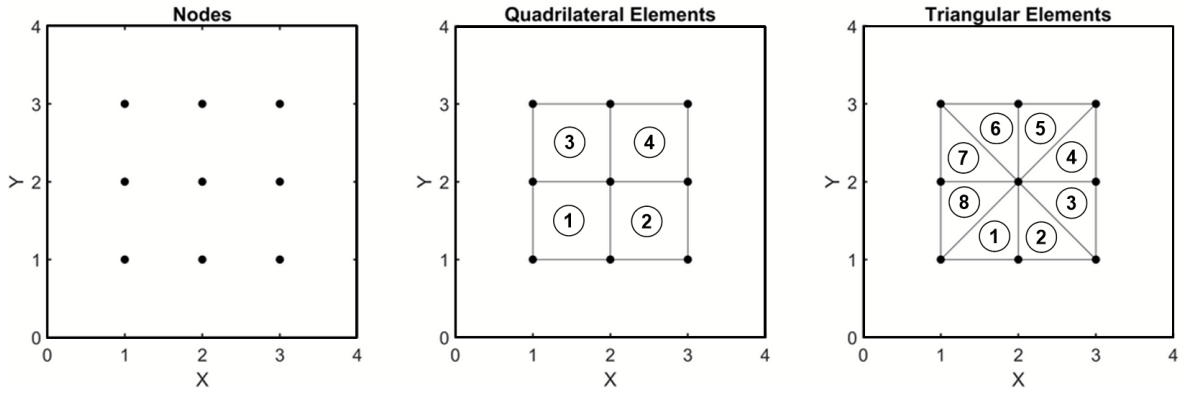

Figure 3.5: Structural nodal discretization for a 2D continuum (left) via quadrilateral (middle) and triangular (right) elements.

Given the study objectives of investigating bridge dynamic behavior under temperature distribution, there are two important criteria for the selection of the reference elements. The element should approximate stress and strain distributions while accepting temperature as loading and it should be compatible with a modal analysis simulation, compatible with a FEM software (ANSYS). Consequently, the selected reference elements are SHELL181, suitable for thin shell structures such as steel girders, and LINK180, suitable for cables and bracings in bridges.

SHELL181 is a four-node element with three degrees of freedom in translations and three degrees of freedom in rotation (ANSYS, 2024). The degrees of freedom are related to the three-dimensional continuum (Cartesian axes). This element is suitable for linear, large-strain deformations caused by pressure or temperature. Loading is applicable in the four corner nodes (denoted I, J, K, and L in Figure 3.6). As a single-layer 2D element, the thickness can be assigned to the model depending on the component it describes, such as flange, web, deck, etc. The second element is LINK180, a two-node uniaxial element with three degrees of freedom at each node, allowing translation in the x, y, and z directions. It is a tension and compression 3D element, supporting temperature loading in the nodes (ANSYS, 2024).

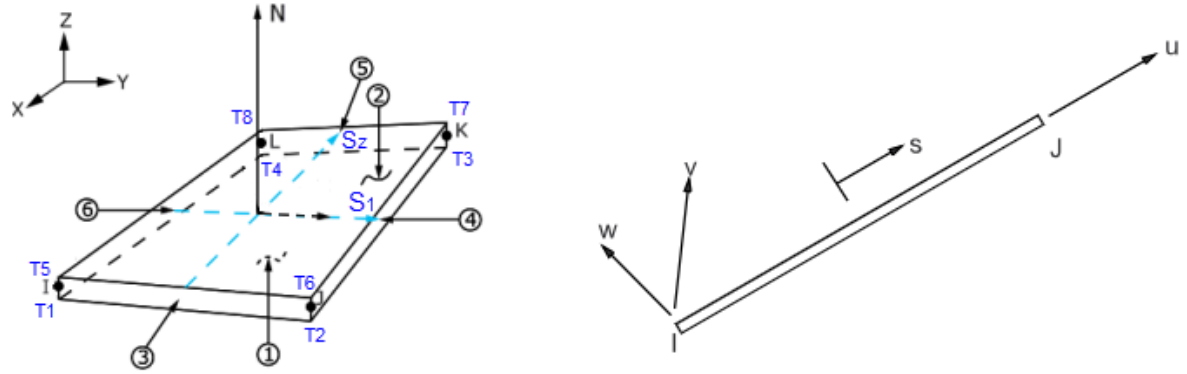

Figure 3.6: SHELL181 geometric model (left); LINK180 geometrical model (right) (ANSYS, 2024).

To define each bridge component independently, material profiles are assigned independently of each other. The input values are the density of the material (assumed to be isotropic), Young's modulus (resistance to elastic strain under induced stress), the Poisson ratio (expansion relative to the compression in the perpendicular direction expressed as the ratio of transverse strain to axial strain) and the isotropic thermal expansion coefficient (the rate at which the material expands or contracts relative to the change in temperature). The output of the reference elements is the nodal displacement, and the stress and strain distributions, categorized into the mechanical and thermal profiles. The modal analysis is compatible with both elements if the temperature is considered static loading.

The matrix-vector representing the element equations about the displacement and rotation is combined with the load vectors (the temperature distribution). Solving these systems of equilibrium equations requires the definition of the boundary conditions for the model. The boundary conditions in the structural analysis relate to the restriction of the movement specifically in the support locations for the displacement and rotation. There are four major conditions for the boundary conditions; (a) fixed support restricting movement in all translational and rotational degrees, (b) pinned support restricting translations while allowing rotation degrees, (c) roller support allowing one translation degree while restricting translation and rotation of another axis, and (d) no support conditions where translation and rotation is unrestricted (Figure 3.7). The selection process is assisted by the ANSYS toolkit and previous FEA studies of the same bridge (Marchenko et al., 2024).

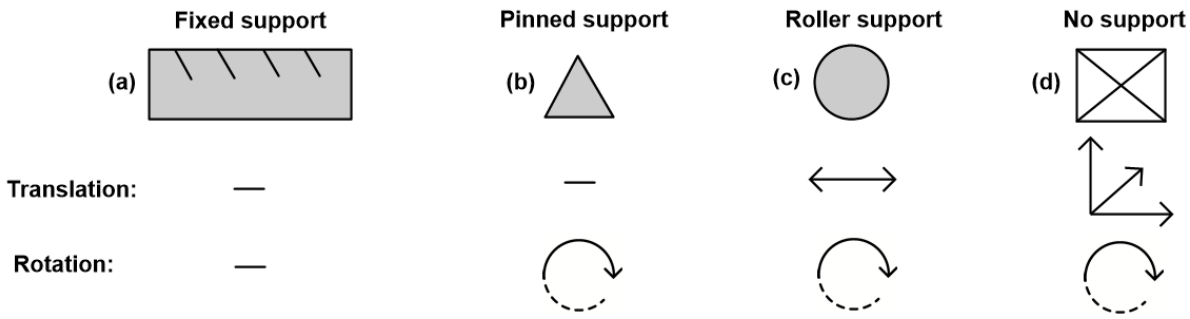

Figure 3.7: Support location configuration (a-d) described in terms of translational and rotational degrees of freedom.

Nonetheless, uncertainties for boundary conditions such as the support type and location, and component stiffness require model updating. The formulation of an objective function is necessary to ensure a good-fitting for the finite element model with the study case observations. The objective function is set to reduce the error between field data and FEA results to less than 10%. The field data dynamic properties for the model updating in this report concern the reference scenario selected in the temperature data analysis (Section 4.1).

Achieving the target accuracy requires sensitivity-based model updating, which includes an iterative process of varying the bridge parameter values and optimizing the support location configuration for the model to match the dynamic properties of the real-life behavior. Initially, the bridge support configuration is adjusted manually, aiming for a converging result within the objective function. Then, a sensitivity analysis of the bridge dynamic response to Young's modulus variation is utilized to reduce the error, if the boundary conditions do not satisfy the predetermined criteria.

The second part of the model updating is determining the temperature distribution. In alignment with the temperature data analysis, five different scenarios that resemble the field data measurements exhibit the basis of the temperature distribution. Depending on bridge component geometry and materials, Eurocode provides rough estimates that are not tailor-made distributions, therefore reliability is low (Kromanis et al., 2015). Depending on the number of thermocouples and their spatial distribution in the bridge, the measurements lack complete temperature profiling, therefore the vertical and horizontal distribution is built upon existing knowledge and previous studies.

3.3. Data comparison

Results from the uncontrolled acceleration data are presented and compared with the FEA results. To quantify the interpretation of the data comparison, other relevant comparative studies have used methods that depend on the nature of the study and the compatibility of the data with the testing tools. Two main indicators are selected to determine the accuracy of the results; one modal-based and one statistical-based. The evaluation of the Modal Assurance Criterion (MAC) is used to quantify the similarity of model prediction of mode shapes to real mode shapes from the testing campaign (Ren et al., 2004; Mao et al., 2019). As shown in Equation 3.1, MAC is an indicator of the correlation between two modal shapes, where ϕ_o and ϕ_e are the mode shape vectors being compared.

$$MAC(\phi_o, \phi_e) = \frac{\left|\phi_o^T \phi_e\right|^2}{(\phi_o^T \phi_o) \cdot (\phi_e^T \phi_e)} \quad \text{(Eq. 3.1)}$$

The second indicator is Root Mean Square Error (RMSE) in Equation 3.2. It is a statistical measure indicating the magnitude of error between observed value y_i and simulated values $\hat{y}_i$.

$$RMSE = \sqrt{\frac{1}{n}\sum_{i=1}^{n}(y_i - \hat{y}_i)^2} \quad \text{(Eq. 3.2)}$$

To summarize, bridge response is recorded using a structural health monitoring system of sensors including accelerometers along temperature distribution using thermocouples. The dynamic response is categorized into two environments; a controlled environment to determine the natural frequencies for a reference scenario with the least amount of error and an uncontrolled environment to relate the temperature distribution effects in the bridge dynamic response based on scenario selection. The dynamic response captured in terms of bridge acceleration is transformed to the frequency-time domain via FFT to perform a modal analysis of the bridge. Then, an FE model of the bridge developed in ANSYS is updated by optimizing boundary conditions to match observed frequencies for the reference scenario. Temperature data from the data acquisition campaign from a basis to derive the temperature spatial distribution in the bridge to simulate its response under variable conditions. The frequency analysis results from the FEA are compared to the field data to verify the effects of temperature impact on the bridge by measuring the variance between the pertinent datasets.

4

Case study: UT Campus bridge

The proposed methodology is applied in a pedestrian bridge, as shown in Figure 4.1, located on the campus of the University of Twente, in the city of Enschede, the Netherlands. This bridge will serve as the case study for the comparison of the collected data from sensors in the bridge with the FEA simulations. The bridge was opened to public use in the 1980s, accessible for pedestrians and cyclists. It connects Sintelbaanveld in its western link with Hogekamp on the eastern side, crossing over an artificial pond (4.1c). It is oriented in a northwest-to-southeast direction, while its exposure to the sun changes depending on the season varying with more exposure hours in the summer and less radiation during winter.

(a)

(b)

(c)

Figure 4.1: The UT Campus bridge: (a) side-view, (b) bottom-view, (c) top-view.

The northwestern side is an exemption due to the shadows caused by the extensive presence of trees, while the presence of buildings nearby such as Vrijhof (south) blocks the radiation in the early evening hours, while the Plaza Residence and UPark Hotel (east) block the sun rays in the early morning hours. The exposure of bridge elements also changes with the position of the sun, with the middle girder enclosed in all directions, being the least exposed element to solar radiation. In summer, the sun's trajectory is longer, reflected by the extensive sunny hours and higher temperature gradients in the bridge. In winter, the trajectory is smaller, with the day being shorter and the radiation prevented by the continuous cloudy and rainy weather. Consequently, the temperature gradients are smoother and lower than on summer days. The maximal and minimal solar projection based on the sun's position is given in Figure 4.2 for the two solstices on the 21st of June and on the 21st of December.

(a) (b)

Figure 4.2: Sun trajectories in (a) summer solstice on the 21st of June (b) winter solstice on 21st of December.

In technical terms, the UT Campus bridge is a steel girder and timber deck bridge, spanning 27 meters long and 2 meters wide. The structure is composed of three 27-meter-long IPE600 steel girders and 80x80x5SHS horizontal bracings. The D40 hardwood oak timber deck is sided by a total of twenty-two timber railing posts bolted to the outer girders (Figure 4.3). In 2022, a complete SHM system of sensors was installed in the bridge. Since then, the bridge has been continuously monitored using temperature sensors, accelerometers, strain gauges, and a local weather station. Due to a lack of information about the prior conditions of the bridge when it became operational, visual inspections have necessitated a structural assessment of the bridge. This has provided a ground study for several SHM investigations in the past (Kromanis (2021); Marchenko et al. (2024)) regarding camera-vision testing, long-term data collection, etc.

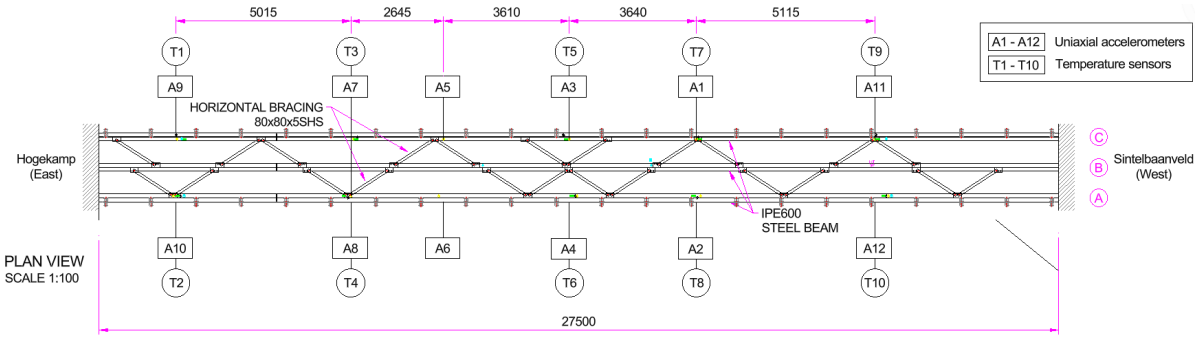

Figure 4.3: Structural top-view drawing of the UT Campus bridge with the locations of installed thermocouples (T-i, i=1,2,...,10) and accelerometers (A-j, j=1,2,...,12).

4.1. Temperature analysis

The UT Campus bridge is exposed to considerable solar radiation due to the low-rise surroundings. The induced temperatures are measured from 10 sensors located in the steel girders, continuously where each measurement is stored on a regular timeframe of 5 to 10 seconds depending on the time delay of system synchronization. The obtained data from one year-long bridge monitoring (Figure 4.4) reveals the fluctuation on a seasonal basis where the cold months from December to April show a fluctuation of temperatures between a minimum of $-5\,°\mathrm{C}$ to a maximum of $23\,°\mathrm{C}$, while summer is characterized by a fluctuation from a minimum of $10\,°\mathrm{C}$ to a maximum of $40\,°\mathrm{C}$. The gaps between July and September as well as November to December are related to some malfunctions in the monitoring system.

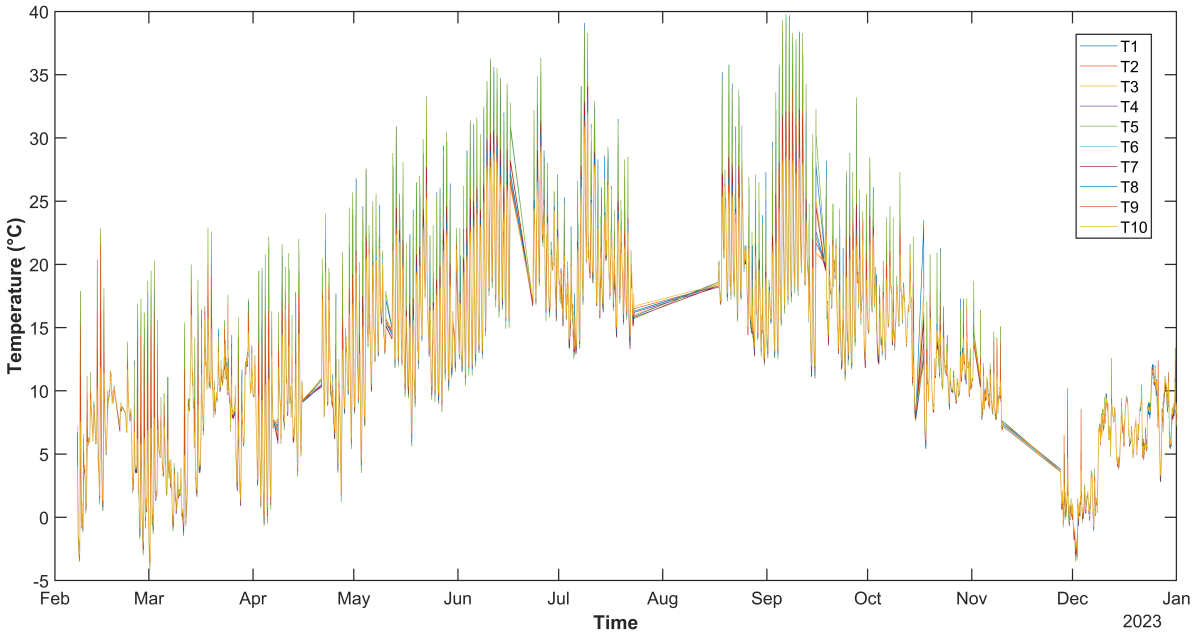

Figure 4.4: Annual temperature measurements from thermocouples (T-i, i=1,2,...,10).

Zooming in on Figure 4.4, specifically on 3 days between 28th February to 2nd March, reveals the actual distribution of temperature temporally and spatially. Figure 4.5 explicates the day-night cyclic change in temperature where the maximal temperatures are recorded in the afternoon while the lowest temperatures are in the early morning hours with the lowest being $-4.1\,°\mathrm{C}$ in the early morning of 1st March. As the sun approaches its zenith, the temperature increases gradually with the sensors of the southeast side (sensors T1-T9) being the ones exposed more to solar radiation. This is reflected by the higher temperature measurements recorded at any time instant between 12:00 am to 17:00 afternoon, with a highly variable temperature distribution recorded at 15:00 with a maximal amplitude of $12\,°\mathrm{C}$.

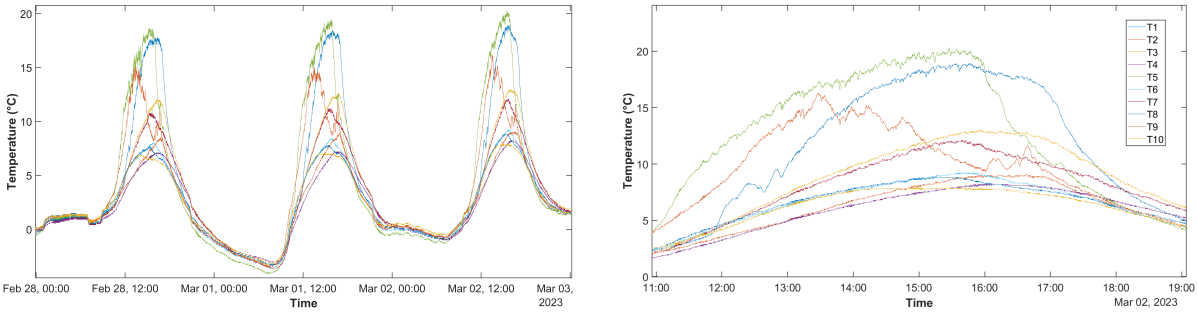

Figure 4.5: Temperature distribution for a high variable three-day period (left) and spring midday (right).

The data was processed so that for each measurement, the biggest amplitude between maximal and minimal measurement was recorded, and the largest standard deviation of the ten measurements was calculated. These two statistical parameters were considered as indicators of the highest variability of temperature distribution in the structure. The higher the standard deviation and the change in amplitude the more temperature varies across the structure, while the reverse is also true and is connected to both low temperatures typical for early winter mornings or equal solar radiation specific for cloudy spring days of mild temperatures. The selected temperature scenarios (Figure 4.7) are: an extremely hot afternoon (Figure 4.6a), an extremely cold sunrise (Figure 4.6b), a cloudy summer afternoon (Figure 4.6c), and highly variable temperature distribution in spring midday (Figure 4.5) and a reference scenario of a cloudy autumn afternoon (Figure 4.6d) with an average temperature of 20 °C.

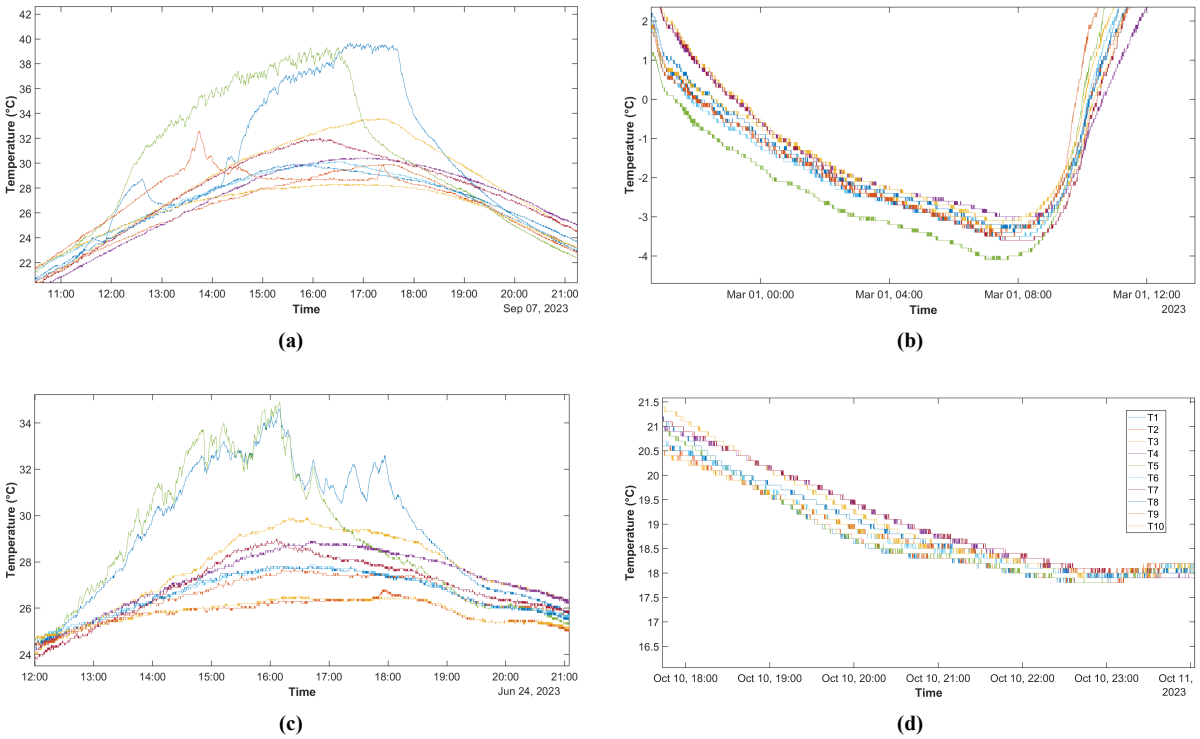

Figure 4.6: Temperature distribution for (a) an extremely hot afternoon, (b) an extremely cold sunrise, (c) a cloudy summer afternoon, and (d) a cloudy autumn afternoon.

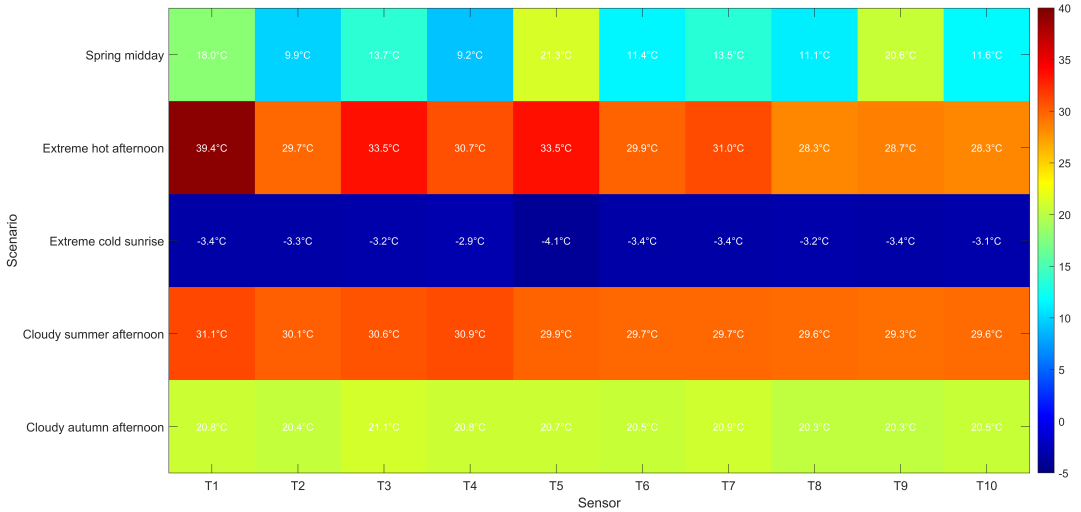

Figure 4.7: Five selected scenarios from one-year temperature monitoring.

4.2. Acceleration analysis

Controlled environment testing is conducted to further explore the natural frequencies of the bridge. This study consisted of a controlled excitation experiment with wireless sensors on the UT Campus bridge, on the 25th of April 2024, a cloudy spring day with an average temperature of 20 °C. A total of four wireless accelerometers were positioned in four points, three being on the quarter, half, and two-thirds span of beam A and one accelerometer in the half span of beam C. Nine consecutive heel drops were performed in a predetermined pattern of walking with a 5 seconds delay to allow the bridge to respond naturally as the excitation energy dissipates after each jump. The force exerted is a result of the free fall of an individual (approximated at 900 N), with no other considerable force of excitation acting upon the bridge. The pattern of the movement and jumping is displayed in Figure 4.8, with the resulting acceleration data plotted in Figure 4.9. The vertical axis (z-axis) is considered the dominant axis of acceleration.

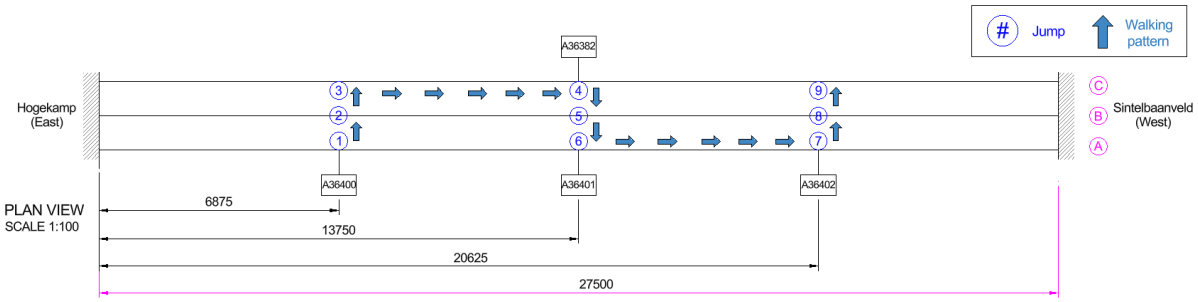

Figure 4.8: Heel-drop controlled experiment layout.

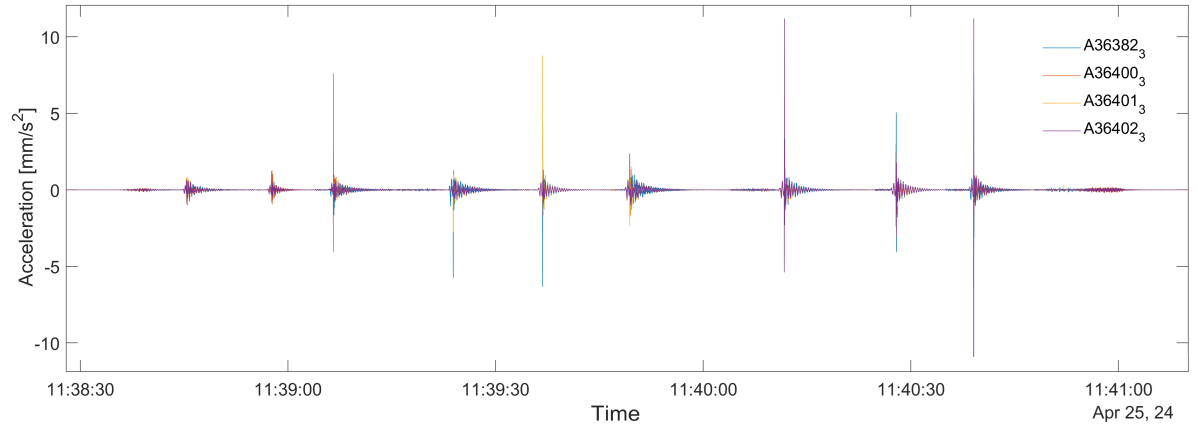

Figure 4.9: Acceleration data of the heel drop controlled experiment.

The FFT is sensitive to short-period measurements (the case of 5 to 10 seconds per heel drop). This can lead to spectral leakage where frequency data is lost due to the infinite periodicity of the signal as treated by FFT. Averaging is performed by dividing the time period into segments computing the power spectral density (PSD) directly from the FFT of each segment (Rogers et al., 1997) via Welch's PSD transformation. This is applied to the acceleration data, with each jump considered separately. The results are aggregated in Table 4.1, which displays the average frequency of all sensors. There were scenarios where the sensors did not record the third mode in jumps 4, 5, and 6 or the second mode in jumps 2 and 8. This can be related to the mode shapes that these frequencies represent and whose excitation location is dominant for the respective jump. Furthermore, the normalized PSD values appeared to change according to the pattern of the heel drop, with the higher accelerations being recorded in a sensor that is the closest to the heel drop location.

Frequency [Hz]	J1	J2	J3	J4	J5	J6	J7	J8	J9	Average
f_1	2.902	2.963	2.983	2.933	2.837	2.94	2.922	2.81	2.913	2.911
f_2	3.764	-	3.75	3.725	-	3.737	3.736	-	3.702	3.728
f_3	8.934	8.955	8.936	-	-	-	8.853	8.88	8.928	8.914

Table 4.1: Frequency estimation from Welch's PSD for nine jumps (J-i, i=1,2,3,...,9).

The testing revealed three mode shapes with an average of 2.911 Hz for the first eigenfrequency, 3.728 Hz for the second eigenfrequency, and 8.933 Hz for the third eigenfrequency. The first mode shape consistently appears in all Welch's PSD plots. The jumps in the middle span of the deck (Figures 4.10b & 4.10h) do not cause any peak that aligns with the second eigenfrequency. It is suspected that this mode is torsional, but it has to be verified by the phase spectrum analysis. The third eigenfrequency appears in the controlled measurements, but not consistently in all nine jumps. Figures 4.10d, 4.10e, 4.10f indicate no peak between 8 and 9 Hz, leading to the assumption that the third mode shape is the lateral or torsional mode shape given the frequency's weaker response for the jumps in the midspan and stronger for the 1/4 and 2/3 jump locations. Nevertheless, the phase spectrum can reveal mode shape patterns to confirm the assumptions about the investigated frequencies.

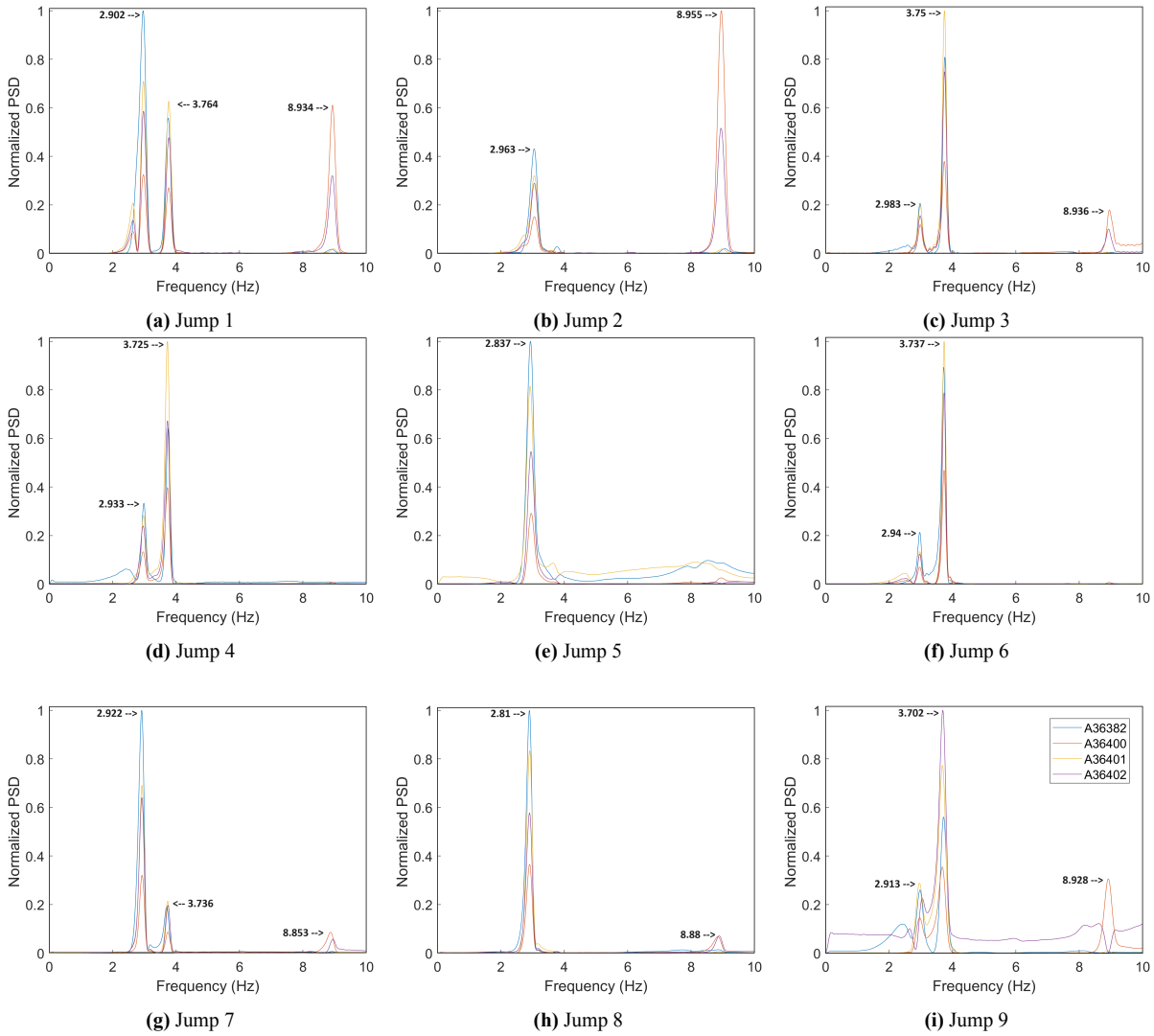

(a) Jump 1 **(b)** Jump 2 **(c)** Jump 3

(d) Jump 4 **(e)** Jump 5 **(f)** Jump 6

(g) Jump 7 **(h)** Jump 8 **(i)** Jump 9

Figure 4.10: Welch's PSD of the controlled experimenting for (a-i) for nine jumps (J-i, i=1,2,3,...,9).

Reflecting upon the jump which conveys the first three frequencies closest to the average is the ninth jump and will be used to illustrate the phase of the frequency for all four sensors. For the first mode in Figure 4.11, there is a negative phase for all sensors (a-d) indicating a synchronized direction of oscillation for beam A. It can be extrapolated that the same behavior characterizes beam C, where the sensor in the midspan is negative and similar to the phase of the opposite sensor in beam A, indicating a vertical mode shape. As for the second mode in Figure 4.11, all the sensors of beam A (f-h) have a negative phase thus the same direction of deflection while sensor A36382 located in beam C is positive. This suggests that the midspans of the two beams are rotated around the y-axis, a characteristic of the torsional mode of shape. Although the comparative system is composed of just the midspan sensors, determining whether the modes are symmetric or not is a matter of accelerometers' symmetrical measurements.

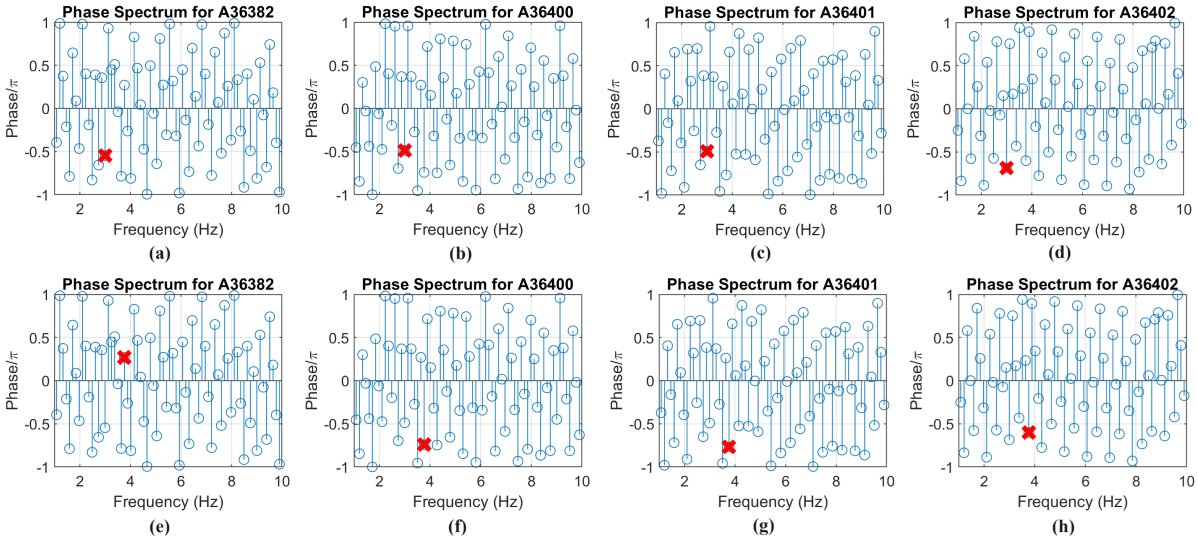

Figure 4.11: Phase spectrum: (a-d) for the first eigenfrequency and (e-h) for the second eigenfrequency.

The Welch's PSD plots from the second jump (Figure 4.10b) with the highest amplitude for the third mode and from the fourth jump (Figure 4.10d) with no peak around the third mode are selected to verify the lateral movement, by analyzing acceleration in x-direction. Figure 4.12a reveals the dominant frequency to be around 9 Hz, while no significant spike is evident around 3 and 4 Hz. On the other hand, Figure 4.12b confirms the previous Welch's plots in the y-direction, where no lateral movement is recorded. If the excitation is in the center of mass of the bridge, the dominant frequency based on the PSD values is the vertical mode shape. In the case of jumps in girder A or C, the torsional mode is the dominant frequency, while the third mode is triggered when the heel drop is distant from the center of mass; where inertia makes the bridge deform laterally due to the angle of the center of mass and the force of excitation.

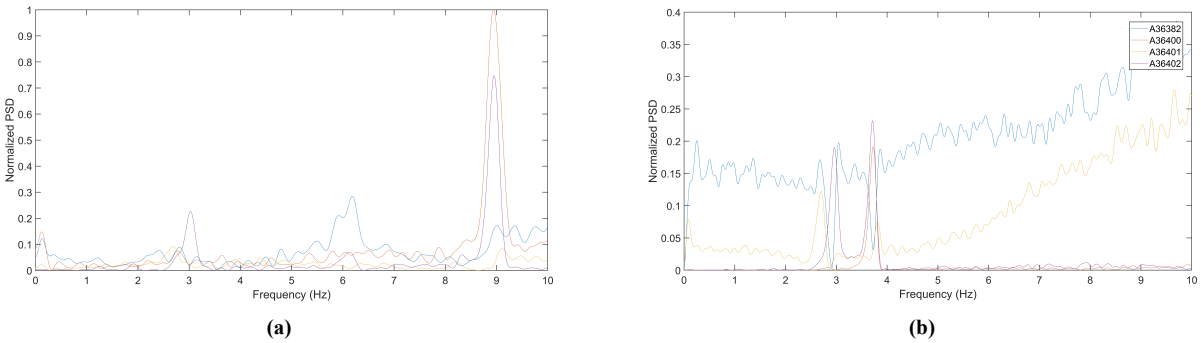

Figure 4.12: Welch's PSD for (a) jump 2 and (b) jump 4 in the horizontal direction (x-axis).

4.3. Finite element analysis

This section elaborates on the investigation of temperature loading effects in the 3D FE model of the UT Campus bridge. The base model of the bridge used from previous studies on the static response of the bridge to various loading (Marchenko et al., 2024) is utilized to conduct a modal analysis of the bridge under temperature distributions built upon the temperature measurements discussed in Section 4.1. The bridge is modeled in ANSYS (2024), a FEM software package specialized in structural and thermal analyses. A programming environment called ANSYS Parametric Design Language (APDL) is used to define the bridge geometry and boundary conditions. The bridge geometry and properties are represented by two materials: steel girders and bracings and the timber deck. These materials are modeled by two reference elements: SHELL181 for girders and timber decking featuring a 4-node element with six degrees of freedom including translations and rotations around three axes and LINK180 for the bracings. These elements are suitable for linear and non-linear stress-strain analysis caused by static or dynamic loading. The elastic modulus of steel is set to 210 GPa and for the timber decking at 9 GPa with a reference temperature of $20\,^{\circ}\mathrm{C}$. Bridge geometry is slightly simplified (Figure 4.13), and a 1/10 mesh ratio is adopted, resulting in 3047 elements connected via 6309 nodes.

The section starts with an explanation of the model updating techniques implicated in the Methodology (Chapter 3). The results are supported by a sensitivity analysis to clarify the rationale behind the proposed changes in the model for future studies. The second section of this chapter focuses on temperature distribution and techniques applied to derive meaningful temperature loading for the bridge based on collected data and a literature review.

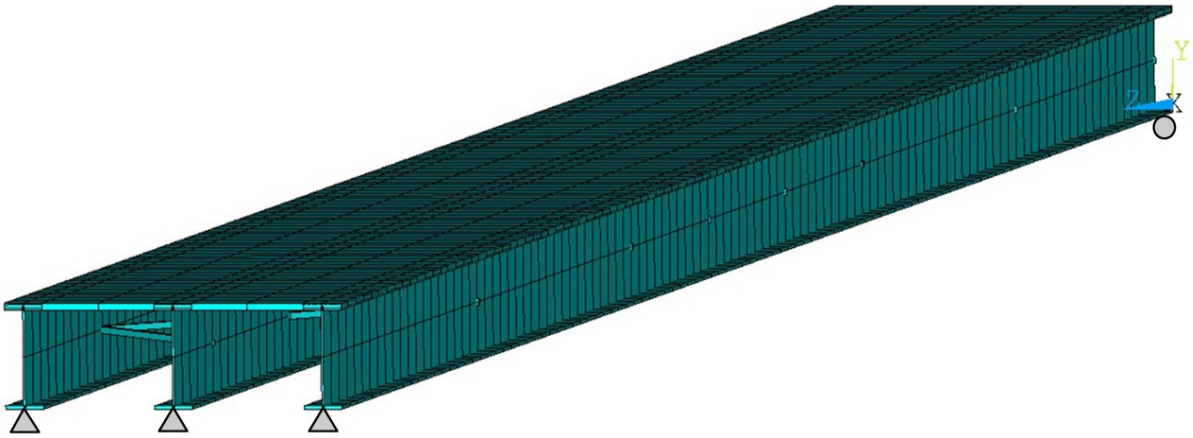

Figure 4.13: FEM of the UT Campus bridge.

4.3.1. Model updating

The model was previously used for static investigations (Marchenko et al., 2024), where the boundary conditions used by these studies are not calibrated to match the dynamic behavior of the bridge in reality. Therefore model updating is a procedure of repetitive trial and error experimenting on the boundary conditions to approximate the FE model dynamic properties as close to the observed frequencies. Model updating is applied to numerical models due to the inherent uncertainty about the structural support conditions or the stiffness of the materials in case of long-service deteriorated structures. For the dynamic model updating, the objective functions consist of modal parameters such as natural frequencies and mode shapes, although the latter is rather complex due to the local variation in long-span bridges. For this study, the objective function is to update the mode so that the first three natural frequencies of the bridge are within a 10% error range from the observed frequencies in the controlled experiment.

Several studies have conducted model updating techniques to match either static or dynamic bridge response, and a general tendency is to start with a sensitivity-based model updating (Brownjohn and Xia (2000); S. Li et al. (2014); Zhu et al. (2015)). This method examines the impact of density and stiffness (Young's modulus) on bridge dynamic properties. The model is iterated manually for different configurations of the boundary or support conditions. The manual iteration is a complex procedure that requires an immense amount of trial and error due to the possibilities of the boundary conditions. There are three girders in the bridge, where each girder has two sides and each side has 7 nodal points where to apply the boundary conditions. There are three possibilities for each nodal point: applying pinned support, roller support, or no support. Considering these primary conditions, the number of trials is beyond computational power (3^{42} trials). Therefore, a manual trial and error procedure starting from a basic configuration of supports is conducted, where pattern recognition depending on the variation of the eigenfrequencies will be used to determine the best fit for the model. The modal analysis was conducted independently of each iteration with a reference temperature of $20\,^{\circ}\mathrm{C}$ so that the results are comparable to the controlled experimental average eigenfrequencies.

Figure 4.14 represents the trial and error procedure. The x-axis represents the configurations, where RR corresponds to roller supports in the selected supports, PP corresponds to pinned supports in the selected nodes, and RP refers to one side of the girder being constrained by roller support and the other with pinned support. The number signifies the node location with '1' being the nodes in the middle of the web, '2' being the nodes in the middle of the top flange, '3' representing nodes in the middle bottom flange, '4' being the nodes in the middle of the web and bottom flange, '5' being the nodes in the middle of the web and the flanges. RR-1 is considered base configuration and the change in simulated results is compared accordingly.

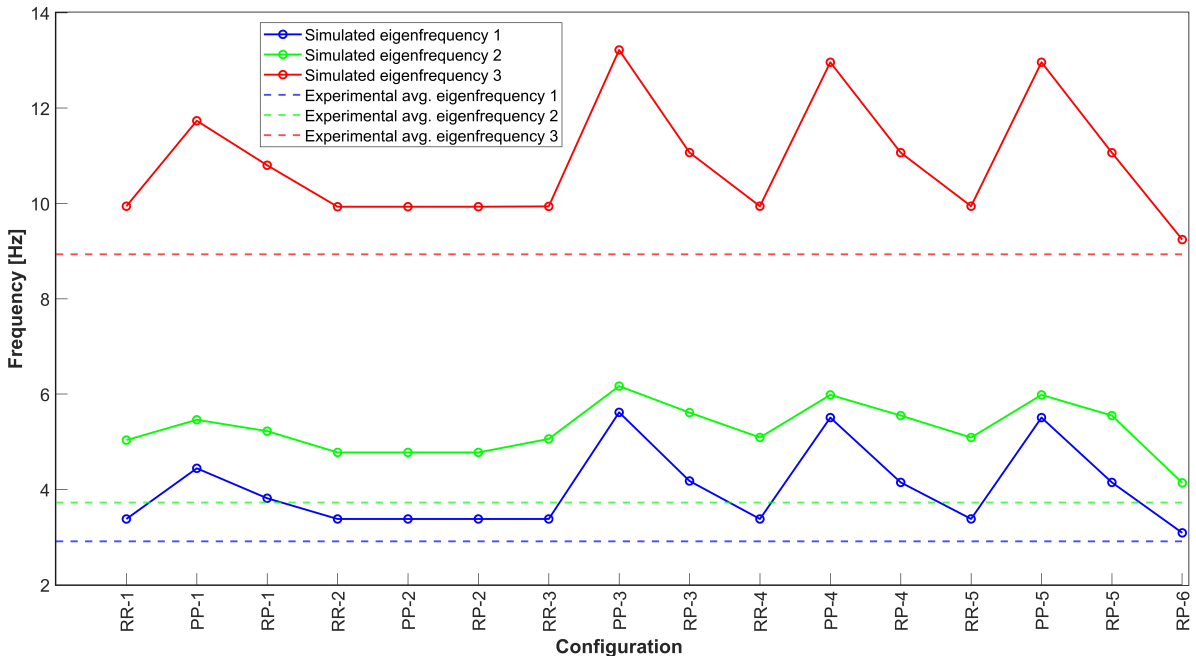

Figure 4.14: Model updating results comparing the sensitivity of the FE model to change between three support configurations (RR, RP, PP) in five different locations of the girder profile.

The last scenario is a specific configuration that resulted as the best configuration with the least deviance from the experimental data and is represented in Figure 4.15. It consists of a predominantly pinned support in the east side, restricting axial movement in the middle web and middle lower flange. The west entrance consists mostly of roller support, allowing uniaxial movement and rotation.

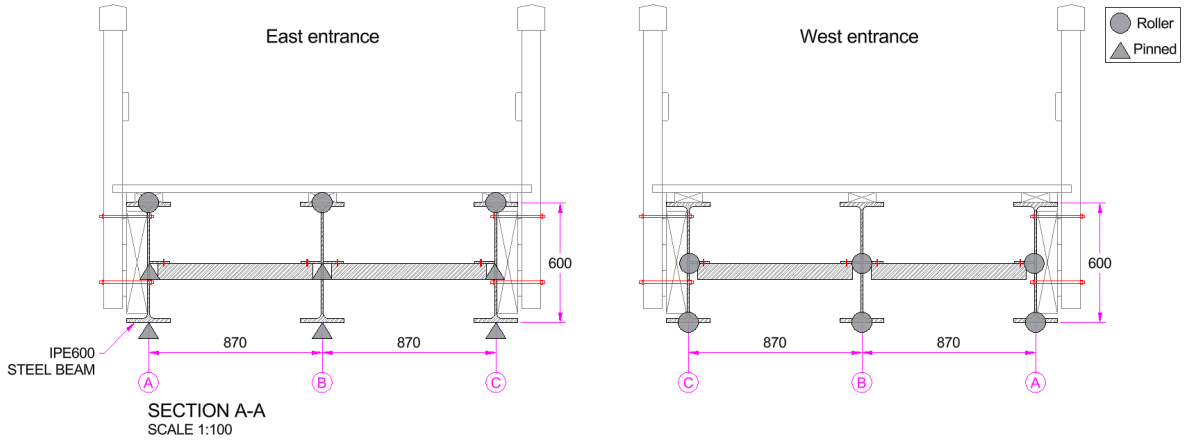

Figure 4.15: Supports configuration (RP-6) in the steel profiles for the east (left) and the west entrance (right).

There is a similar trend for all eigenfrequencies to decrease in any configuration of roller support compared to pinned support. The roller supports allow horizontal movement while restricting vertical movement and rotation. The pinned supports restrict both vertical and horizontal movements while allowing rotation. The increased eigenvalues from roller to pinned supports are related to the resistance to oscillation. More restriction on the supports translates to a higher stiffness-to-mass ratio. This causes the bridge to experience greater vibration because it resists deformation more compared to a less stiffer structure. The configurations in the top flange showed little to no impact (Scenario 2 in Figure 4.14). Therefore, the most contributory support locations were the middle web nodes and the nodes in the middle of the bottom flange, which resulted in the most appropriate configuration with the following results in Table 4.2.

Frequency	Simulated [Hz]	Experimental [Hz]	Error [%]
f_1	3.089	2.911	6.11
f_2	4.138	3.728	10.99
f_3	9.241	8.914	3.67

Table 4.2: Comparison of simulated and experimental eigenfrequencies.

Material properties, such as Young's modulus of steel girders and a timber deck, are among the input parameters considered in the baseline FE model under optimal conditions ($E_{\text{steel}} = 210$ GPa; $E_{\text{timber}} = 9$ GPa). However, the certainty of these values is low due to signs of deterioration observed in the structure, such as excessive rusting in the girders (see Figure 4.1b). To assess the sensitivity of the model to changes in these parameters, the modal analysis results will be compared and updated to minimize errors.

The sensitivity is evaluated based on a 5% incremental change of the primary value highlighted as the optimal conditions in a reduced range of 25% from the reference value for steel girders, timber deck, and both components simultaneously. This range is sufficient to test the reliability of the model to assess the impact of input parameters (Brownjohn and Xia, 2000); implying an apriori damage to the structure to verify changes in the modal parameters and the magnitude of this change to be within a reasonable range of outputs. Increasing the stiffness is impractical because the structure degrades over time, thus limiting the analysis only to the reduction testing. Consequently, the sensitivity results for the steel girder and timber deck are presented in Figure 4.16. They confirmed the findings of other studies as well as the relation between frequency and Young's modulus seen in Equation 2.1.

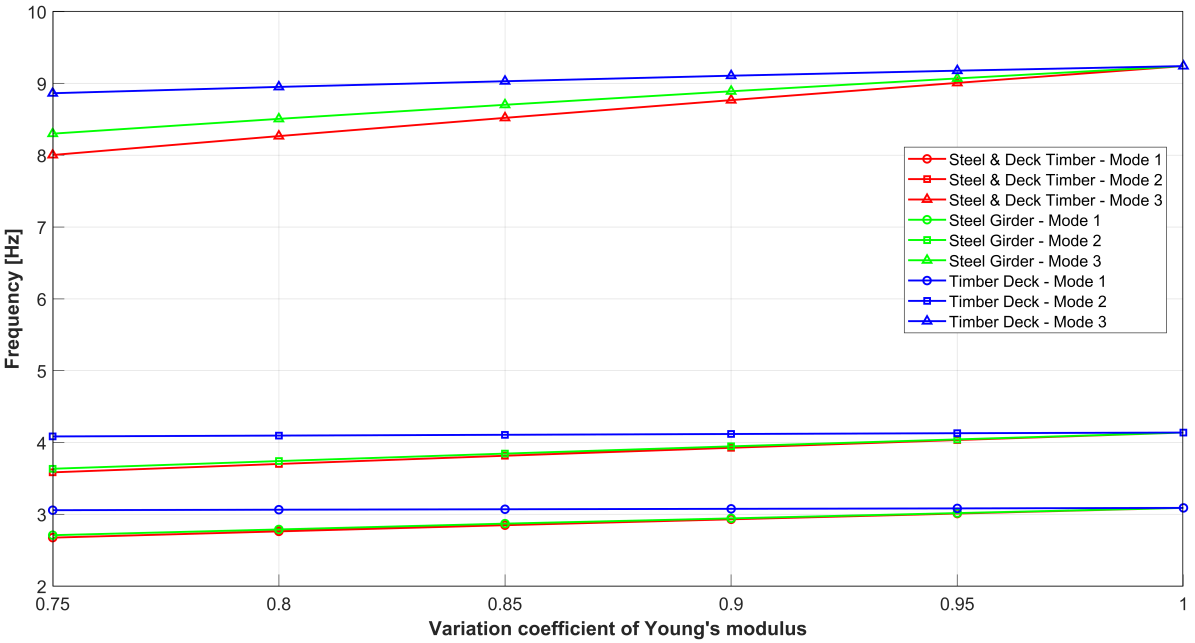

Figure 4.16: Sensitivity of eigenfrequencies relative to Young's modulus variation.

In all scenarios, the Young modulus is directly proportional to the eigenfrequencies; resulting in smaller frequency values in all modes for all damage scenarios. This is related to the tendency of the structure to be prone to more deformation as the stiffness decreases, resulting in fewer vibrations and a smaller frequency. The relative impact of the steel and timber components is derived from the slope of the change. The change in Young's modulus of steel is the main contributor to the change in eigenfrequencies causing a maximum change of 12% for the first and second modes and 10% for the third mode. The decking timber causes a maximum change of 1% in the first and second modes, and 3% in the third mode. These results suggest that changes in steel Young's modulus affect the first and second modes more compared to the impact of timber deck. The latter scenario causes a notable change for the third mode relative to its effect on the first two modes. The higher sensitivity to steel Young's modulus is related to the composition of the structure with the steel girders being the main bearing structure having the biggest volumetric and mass ratio where the initial boundary conditions are applied. The timber deck provides a support surface for pedestrians and cyclists, hence structurally distributing the loads to the girders.

Finally, the results of this sensitivity are used to approximate the bridge's actual conditions by reducing the error in the dynamic parameters. Combining the boundary conditions determined earlier in the chapter, and the scenario with a 10% decrease in the Young modulus of steel and timber deck, the updated simulated results are presented in Table 4.3. The change in error is below the 10% significance threshold determined in the methodology, for the model result to be considered reliable and representative of the bridge's actual response.

Frequency	Simulated [Hz]	Experimental [Hz]	Error [%]
f_1	2.929	2.911	0.62
f_2	3.957	3.728	6.14
f_3	8.758	8.914	-1.75

Table 4.3: Comparison of updated simulated and experimental eigenfrequencies.

This model updating section is concluded by the respective plots from ANSYS for three mode shapes, which correspond to the first symmetrical vertical (VS1) in Figure 4.17b, first symmetrical torsional (TS1) in Figure 4.17c, and first asymmetrical lateral (LA1) in Figure 4.17d respectively. The plots are the result of a prestressed modal analysis conducted for the reference scenario where a constant $20\,^{\circ}\mathrm{C}$ is applied to all nodes (Figure 4.17a). A prestressed modal analysis is performed to account for the impact of temperature distribution in the bridge modal parameters. Initially, a static analysis is conducted that solves the system with temperature considered as the input force on the nodes. Consequently, the thermal strain is calculated based on the elongation of the steel and timber profiles. The model saves the stress and strain distribution and applies modal analysis over these conditions.

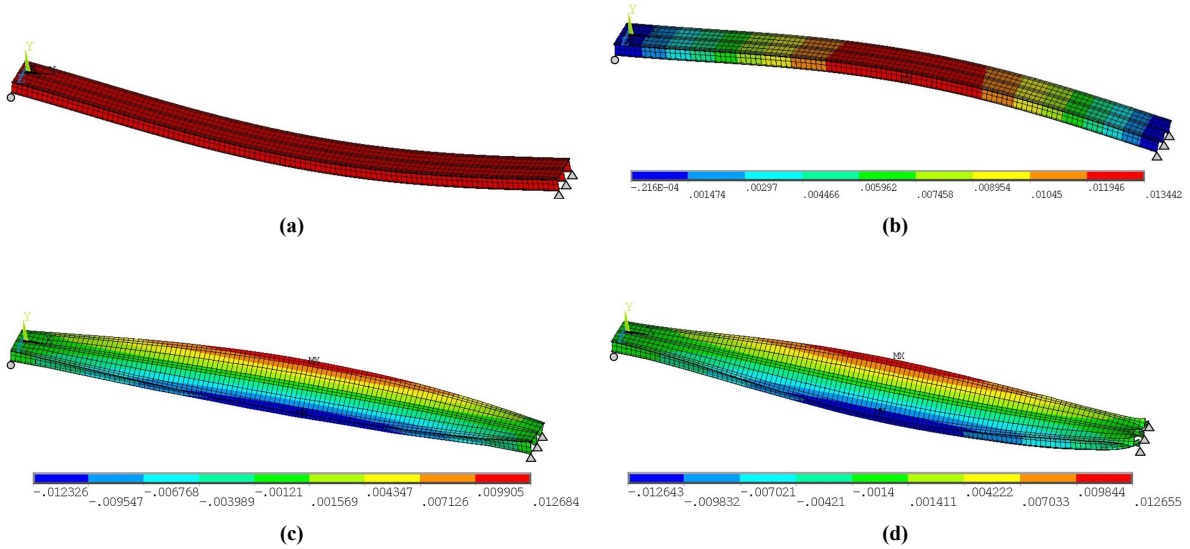

Figure 4.17: FEA results for (a) temperature distribution for a cloudy autumn day, (b) first vertical mode shape (c) first torsional mode shape, and (d) first lateral mode shape.

4.3.2. Temperature distribution in FEM

The primary source of input for the temperature distribution is the temperature analysis conducted in Section 4.1. However, the historical data is not sufficient to describe the temperature distribution in all three dimensions of the bridge, as they are measurements of sensors attached an the bottom flange of the steel girders, thus describing the thermal conditions as a 2D profile of the bottom surface of the bridge. Determining a temperature distribution pattern is a challenging task. The Eurocode includes three bridge models; steel, concrete, and composite decks (Eurocode, 2003). There is no direct approximation for the steel girder bridge with timber decking that is described in the existing Eurocode and National Annexes. Building assumptions upon either of these models does not fit the study case as the UT Campus bridge is a composite structure of timber decking and steel girders, therefore the temperature distribution is modeled based on a literature review of empirical data.

Several studies have conducted transient heat analysis to quantify the temperature distribution in the vertical direction or across the bridge cross-section. Poudel et al. (2024) conducted a parametric study on the effect of temperature gradients on the modal parameters of a composite bridge girder. The girder consisted of an SM355 steel I-beam and a concrete deck. The study revealed that both numerical and experimental data confirm a change of $5\,^{\circ}\mathrm{C}$ to $10\,^{\circ}\mathrm{C}$ across the vertical cross-section depending on the air temperature; with higher (summer) temperatures causing the steeper gradients, and lower gradients representing cloudy colder weather.

Guo et al. (2023) investigated temperature gradient zoning of unpaved steel profiles for steel girders similar to the UT Campus bridge. The maximum temperature difference between the top and bottom flanges reached 11 °C, for the measurement recorded when the sun is in its zenith. Both studies stress the importance of the context of the measurement, specifically the time and the surroundings of the measurement which determines whether the gradient is maximal or not. These studies provide insights into the range and localization of temperature distribution, but it is difficult to extrapolate a definite temperature distribution in scenarios when the temperature is known for one part of the steel profile. Wang et al. (2016) work on thermal behavior analysis of concrete bridges, elaborated on the vertical temperature profile in terms of linear and exponential functions, where the profile is determined by elongation coefficients and a constant term representing the change between maximal and minimal temperature across the profile. Depending on the scenario, the gradient between maximal and minimal temperatures varies with the context. Having the gradient calculated per unit length of the bridge simplifies the model to a 2D temperature profile.

This study utilizes the latter approach by determining the constant term using reference temperature values depending on the weather conditions which are set to vary between three different scenarios as presented in Figure 4.18. The first scenario (Figure 4.18a) assumes a uniform distribution across the steel profile and represents sunrise on cloudy and rainy days where the solar radiation is not strong and heat convection is slow, leading to uniformly distributed temperature. Figure 4.18b characterizes the temperature gradient of cloudy afternoon days and clear weather mornings where the sun heats the illuminated areas more than those in the shadow. The last scenario ((Figure 4.18c) refers to the midday and afternoon cases typically in the late spring and summer days, where the sun's rays exert the strongest radiation. As for the timber decking, the aforementioned studies highlight the distribution of the plates or decks to be more uniform as the solar radiation is continuous throughout the day compared to the girders underneath. In this study, the temperature of the deck is determined by linearly varying the temperature between the two sides of the bridge.

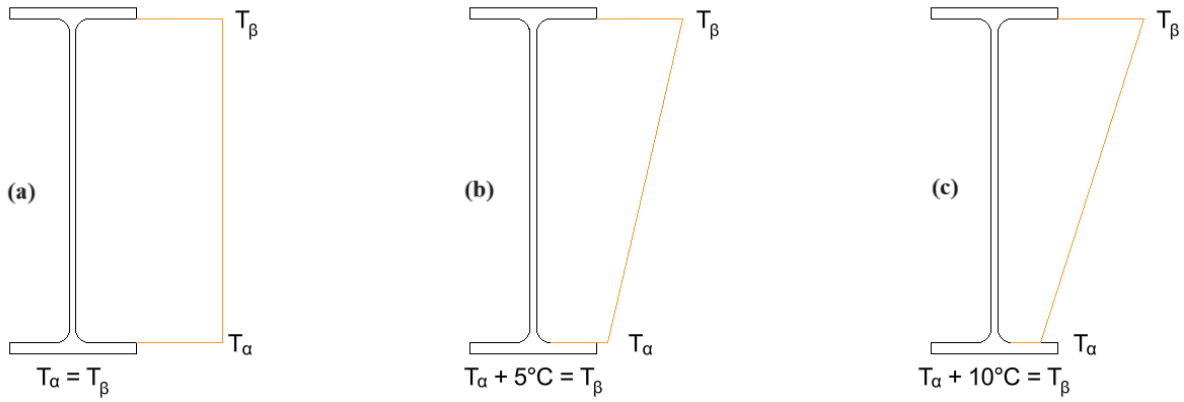

Figure 4.18: Vertical temperature model for (a) uniform distribution, (b) linear distribution with a maximal amplitude of 5 °C, and (c) linear distribution with a maximal amplitude of 10 °C.

The volumetric temperature distribution model is based on a two-sided model, where the input temperatures are defined by 8 nodes, which distribute the temperatures proportionally across the three axes (Figure 4.19). The measurements selected in Section 4.1 include the bottom flange of the steel girders, resulting in the temperature input for the bottom nodes (T5–T8), and necessitating the determination of the temperature for the upper flange. The difference between the top and bottom nodes is determined from an extrapolation of the temperature variation of reviewed studies and assumptions, elaborated in earlier this section.

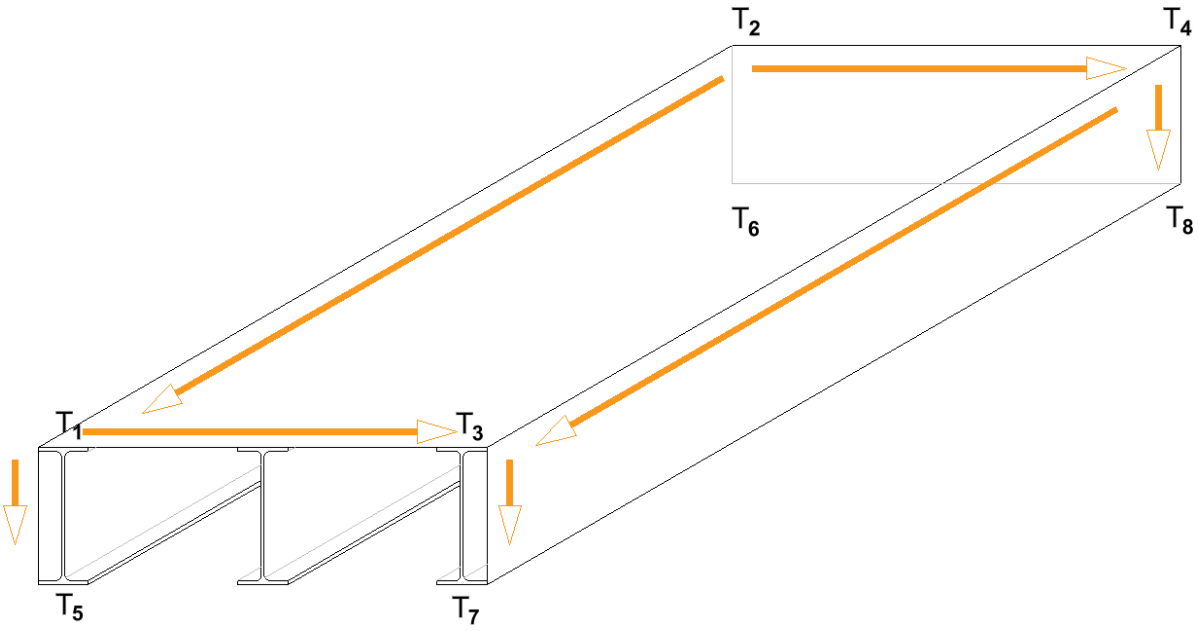

Figure 4.19: Volumetric temperature distribution model.

The five scenarios selected from the historical measurement are adapted following the findings of the aforementioned studies to determine the temperature profiles. Those scenarios are plotted in Figure 4.20, with the arrows representing the temperature spread based on the location of the sun, are:

(a) is SCN I or the baseline scenario used in the model updating section. It simulates a cloudy autumn afternoon where the temperature is uniformly distributed on the bridge.

(b) represents SCN II, a high-variable temperature where the maximal temperature difference is $21\,^{\circ}\mathrm{C}$. Since it is spring midday, the area under direct solar radiation is modeled by a vertical change of $10\,^{\circ}\mathrm{C}$ corresponding to the vertical temperature model (Figure 4.18c), compared to the opposite side, with a change of $5\,^{\circ}\mathrm{C}$ (Figure 4.18b).

(c) refers to SCN III and regards extreme weather conditions in summer. It represents an extremely hot afternoon where the deck and top flange temperature reaches a maximum of $50\,^{\circ}\mathrm{C}$, which linearly decreases towards the west as the radiation angle becomes acute.

(d) relates to SCN IV and corresponds to an extremely cold early morning, where the temperature is uniform across the structure with a temperature of $-3.3\,^{\circ}\mathrm{C}$.

(e) outlines SCN V, which is a cloudy summer afternoon when the sun is approaching the west, and the deck is $5\,^{\circ}\mathrm{C}$ (Figure 4.18b) hotter than the bottom of the girders. The clouds make the heat scatter evenly with a small gradient in the vertical direction.

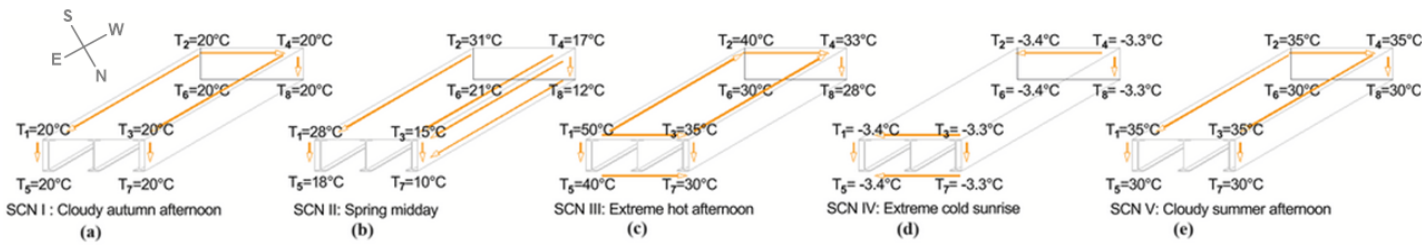

Figure 4.20: Temperature distribution in FEM for (a-e) representing SCN I to SCN V.

5

Results

This section concludes the approach elaborated in the methodology by displaying the results from the uncontrolled acceleration measurements corresponding to the five selected scenarios in Section 4.1 alongside the FEA simulations for the distributions derived in Section 4.3.2. A comparison between the observed and simulated results is conducted, focusing on key dynamic parameters such as natural frequencies and mode shapes via statistical error indicators. The comparative study aims to verify any discrepancies between measured and simulated data, by identifying possible sources of errors and by highlighting limitations of FE modeling in aiding engineers to evaluate bridge performance.

5.1. Scenario-based acceleration data

The selected acceleration data are pre-processed by detrending and smoothening filters to reduce noise and allow for a feasible understanding of the acceleration data for each sensor. Figure 4.9 displays the acceleration measured in the same time instant across the bridge by representing a bicycle cycling east-to-west in the afternoon of a cloudy autumn day.

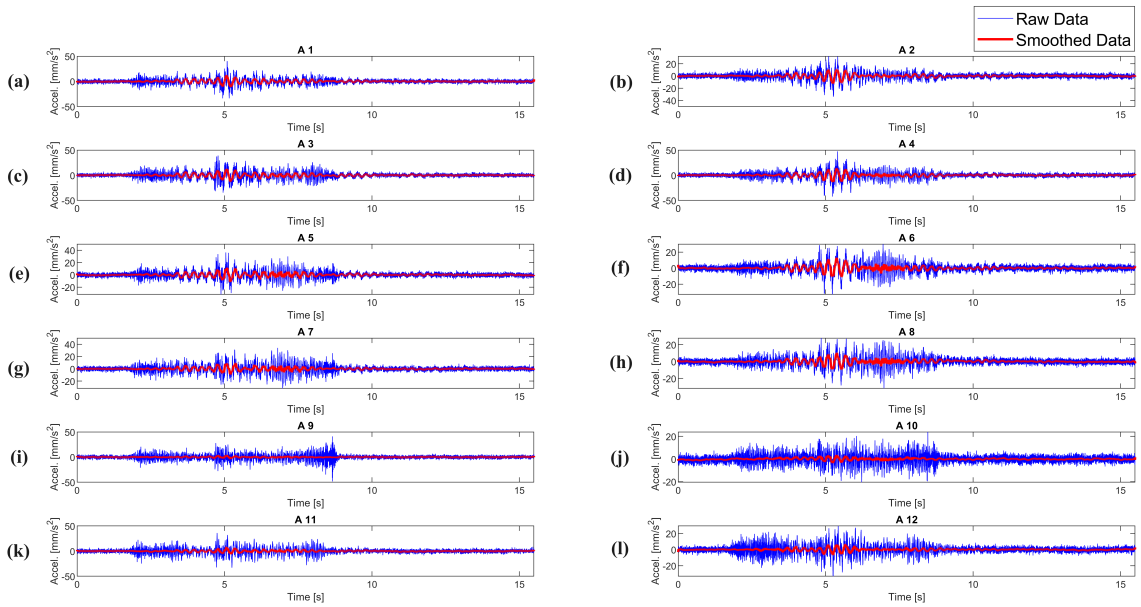

Figure 5.1: Acceleration data of a cyclist for (a-l) from accelerometers (A-i, i=1,2,3,...,12).

A FFT is performed to extract the main frequencies from the acceleration-time domain. For a higher resolution, Welch's method is utilized to reduce spectral leakage by dividing the data into overlapping segments and then averaging to provide a smoother PSD graph. The results are plotted in Figure 5.2. The peak-picking method is used to determine the natural frequencies denoted in each Welch's PSD graph and plotted as a percentage change in Figure 5.3.

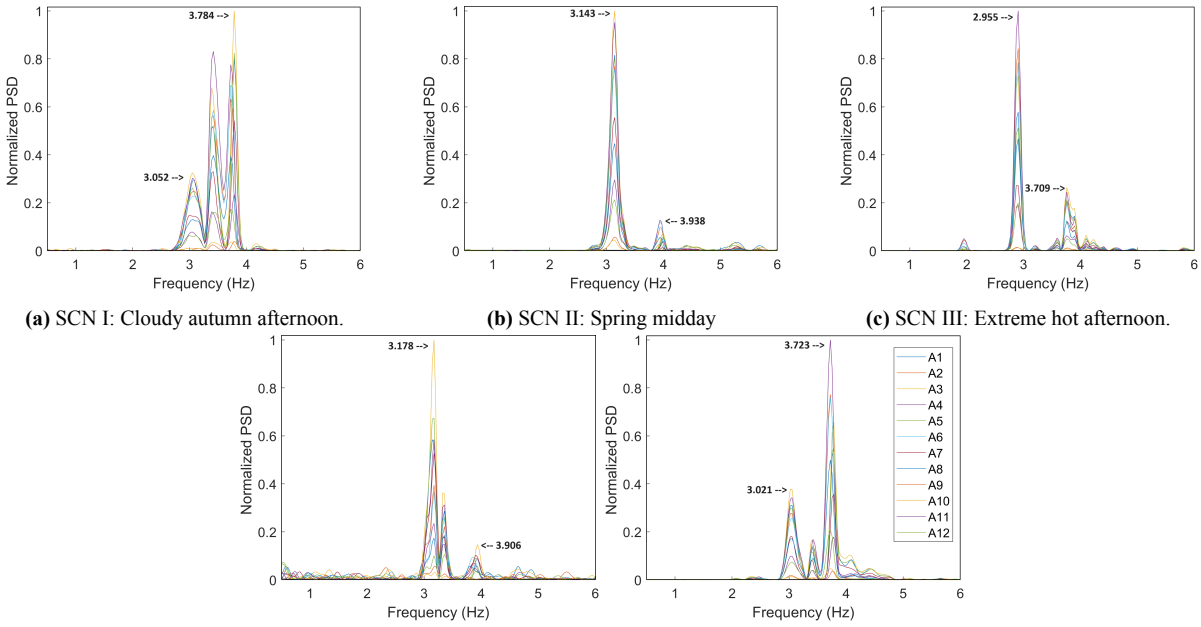

(a) SCN I: Cloudy autumn afternoon. **(b)** SCN II: Spring midday **(c)** SCN III: Extreme hot afternoon.

(d) SCN IV: Extreme cold sunrise. **(e)** SCN V: Cloudy summer afternoon.

Figure 5.2: Welch's PSD of the scenario-based acceleration data for (a-e) from SCN I to SCN V.

Figures 5.2a, 5.2d & 5.2e, reveal peaks in-between the selected first and second eigenfrequencies. These cases signify the resonance in the bridge, where a pedestrian walking frequency matches with the first eigenfrequency of the bridge. Despite the application of the selection criteria to consider only cyclist crossings and avoid resonant peaks caused by pedestrians, the measuring system saves the acceleration recording based on threshold criteria. This threshold criterion starts recording once the bridge exceeds a minimal acceleration threshold and continues to record until the energy of oscillation decays (damping). The measurement may have recorded a pedestrian and cyclist crossing over simultaneously, resulting in resonance.

Figure 5.3 illustrates a tendency for the eigenfrequency to change relative to the temperature variation. Except for the spring sunrise, which depicts an increase in frequency value for the second mode shape (as a result of the nonlinear deformation in the structure), there is a clear trend for the eigenfrequency to decrease as the average temperature in the structure increases, with a maximum change of 7% for the first mode and 6% for the second mode.

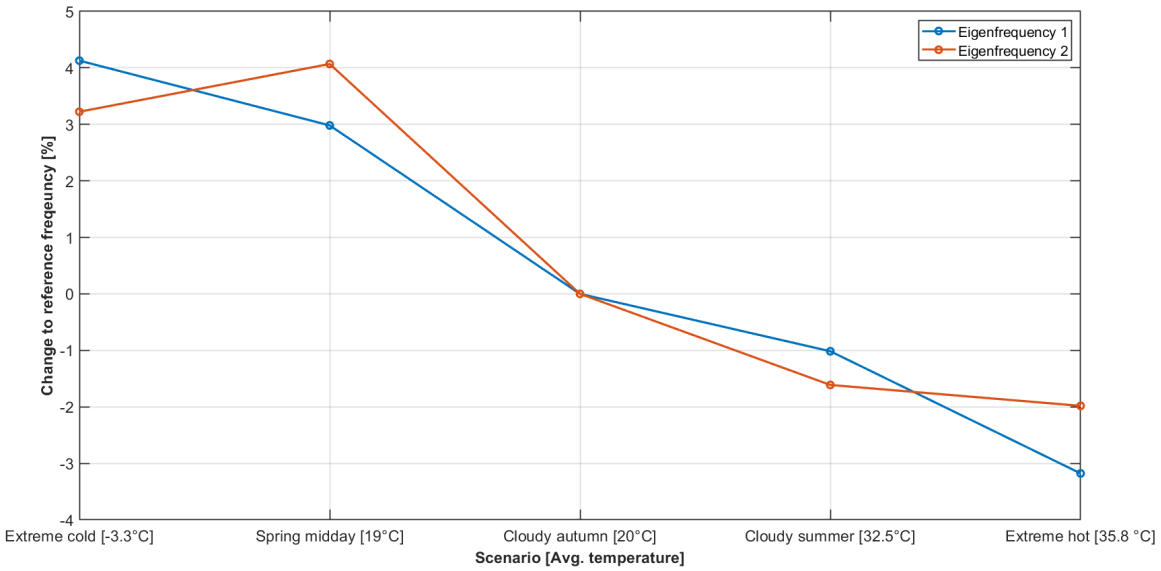

Figure 5.3: Percentage change of observed eigenfrequencies relative to cloudy autumn afternoon.

The mode shapes are related to the identified eigenfrequencies and the spatial distribution of amplitudes of these frequencies. Welch's PSD charts are composed of data from all sensors which are distributed in two beams of the structure namely Beam A and Beam C from Figure 4.3. Extracting the PSD values from each accelerometer provides a distribution of the amplitudes of a given frequency for 12 unit-length nodes of the bridge. The PSD values are normalized to allow for easier comparison between different modes. However, determining the amplitude is not enough to describe the bridge oscillations. Since vibration is a dynamic process, any representation of a mode shape is a snapshot of the vibrating structure and is dependent on the phase of the oscillation. It refers to the angle component describing the oscillations synchronization; in this scenario of the oscillations of the two beams.

Figure 5.4a represents the first modal shape of the bridge which corresponds to a symmetrical first vertical mode shape. Figure 5.4b represents the second mode shape of the structure represented as a symmetrical first torsional modal shape. In the first mode shape the positive phase is reflected by positive values of PSD values while in the second modal shape, the accelerometer installed in beam C had a negative phase causing the torsion around the y-axis. The same pattern is observed for all scenarios, where apart from the change in amplitude, the first and second modal shapes are first vertical (VS1) and first torsional (TS1) respectively. Since all the sensors used are uniaxial, any lateral displacement is not recorded. Despite the frequency that might be predicted in the frequency domain, a mode shape is hard to configure, thus it is not considered in the result processing. The mode shapes for the remaining scenarios can be found in the Appendix A.2. These configurations assume fixed supports for the beams, thus there is no rotation for the boundary conditions, which are to be investigated in the FE model of the bridge.

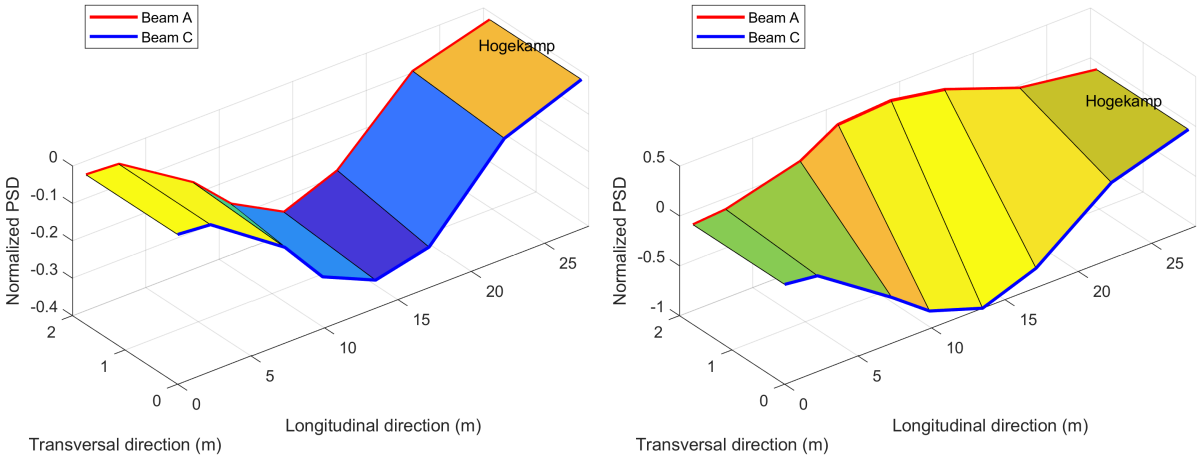

(a) VS1 = 3.052 Hz **(b)** TS1 = 3.784 Hz

Figure 5.4: Scenario-based results of the cloudy autumn afternoon for (a) first symmetrical vertical and (b) first symmetrical torsional mode shape.

5.2. FEA results

The simulation results of the prestressed modal analysis conducted in ANSYS display a narrow range of fluctuation between the eigenfrequencies of each scenario with a maximum fluctuation of 0.03% for the first eigenfrequency and 0.07% for the second eigenfrequency. Therefore, the change in percentage relative to the reference scenario is plotted in Figure 5.5 to elucidate the general trend of change in relation to the average temperature in the structure, followed by an explanation of the results difference based on thermal strain distribution.

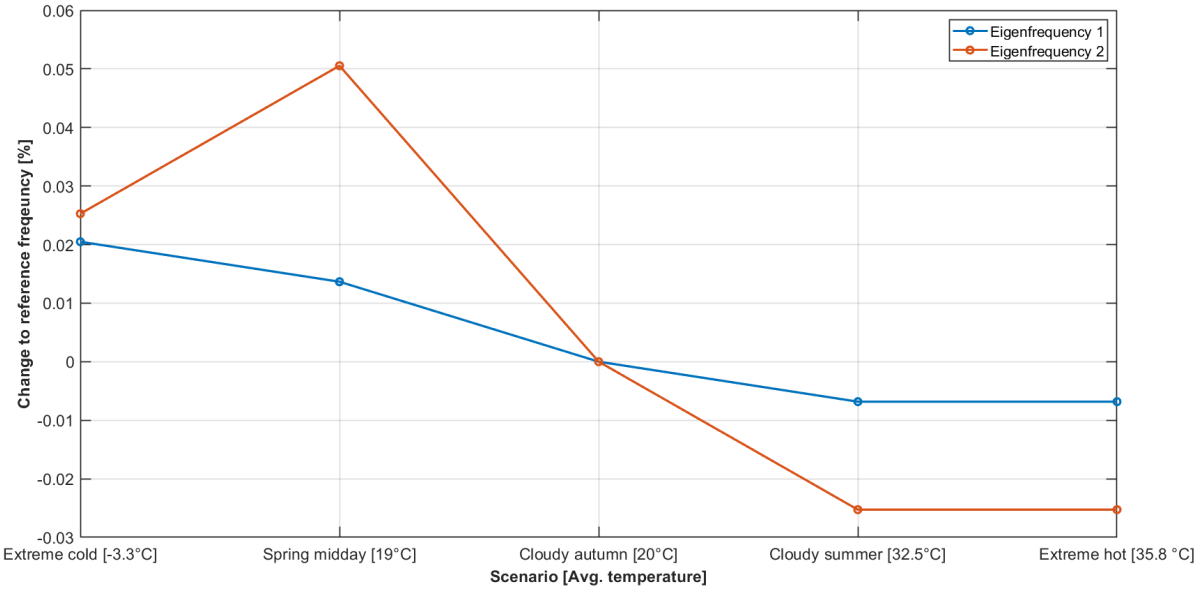

Figure 5.5: Percentage change of simulated eigenfrequencies relative to cloudy autumn afternoon.

Figure 5.5 displays different patterns for two simulated mode shapes. The first and second modes have a decreasing trendline as the average temperature of the structure increases, which is related to the change in the stiffness of the structure. As discussed earlier in Section 2.2, an increase in temperature causes a reduction the Young's modulus. The structure is less stiff and is prone to extensive deformation in terms of strain than to vibration. The same pattern was noticed in the observed eigenfrequencies in Section 5.1. However, there is an incongruous jump from the extreme cold scenario to the high variable temperature distribution (spring midday), similar to the observed eigenfrequencies trendline of the second mode. The imperative of 'the lower stiffness due to higher temperature' would anticipate a smaller frequency for the spring midday scenario. Nevertheless, the latter scenario features a complex temperature distribution, with a maximal amplitude between maximal and minimal temperature of 21 °C (Figure 4.20). This non-uniformity of the temperature gradient, causes some parts of the bridge to expand or contract differently, depending on the thermal strain distribution. The assumptions made in the observed frequencies about the thermal strain can be investigated by utilizing the FEM tools of the thermal analysis. A comparison between the thermal strain of the bridges under extreme cold in Figure 5.6a and high variable conditions in Figure 5.6b, confirms the asymmetry of thermal strains in the second scenario. The uniformity and magnitude of thermal strains in the first case give predictable behavior to torsional deformity, while the regionality of high and low strain values in the second case redistributes the internal forces and increases the torsional resistance for the colder parts of the bridges.

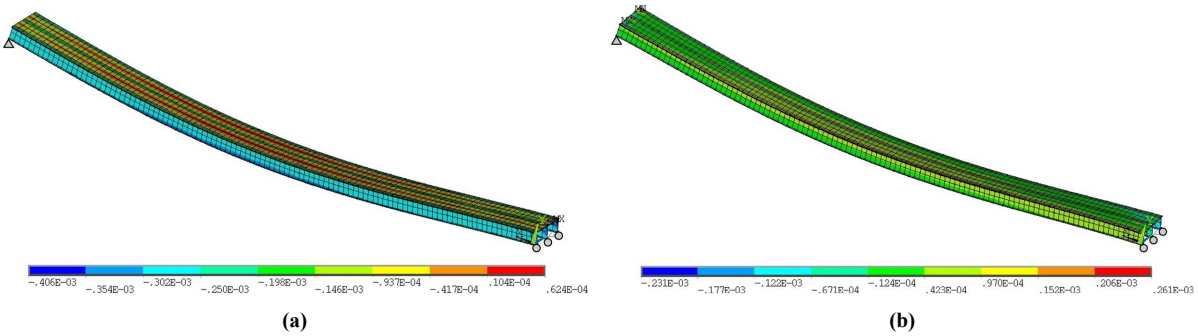

Figure 5.6: FEA results of thermal strain distribution for (a) extreme cold sunrise and (b) spring midday.

Conclusively, the automatically animated mode shapes from ANSYS are in line with the FEA results from the observed frequency phase spectrum. The results for the reference scenario are illustrated in Figure 5.7, with the first mode as the first symmetric vertical (VS1) and the second mode being the first symmetric torsional (TS1). The mode shapes for the other scenarios can be found in Appendix A.3.

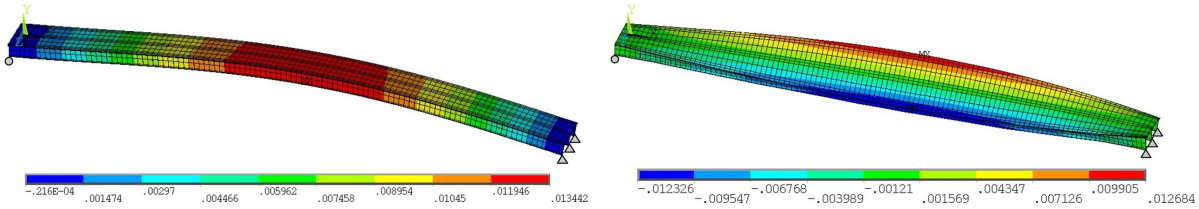

(a) VS1 = 2.929 Hz **(b)** TS1 = 3.957 Hz

Figure 5.7: FEA results of the cloudy autumn afternoon for (a) first symmetrical vertical, and (b) first symmetrical torsional mode shape.

5.3. Data comparison

The results from Section 5.2 in terms of simulated frequencies are weighted relative to the observed frequencies derived from Section 5.1. A cumulative table for the results is given in Table 5.1, where the relative error between the compared frequency values is calculated to verify the change in trend for the FE model response to the change in temperature distribution.

Scenario	**Simulated f_1 [Hz]**	**Observed f_1 [Hz]**	**Error [%]**	**Simulated f_2 [Hz]**	**Observed f_2 [Hz]**	**Error [%]**
Extreme hot afternoon	2.929	2.955	0.88	3.956	3.709	6.66
Cloudy summer afternoon	2.929	3.021	3.05	3.956	3.723	6.26
Cloudy autumn afternoon	2.9292	3.052	4.02	3.957	3.784	4.57
Spring midday	2.9296	3.143	6.79	3.959	3.938	0.53
Extreme cold sunrise	2.9298	3.178	7.81	3.958	3.906	1.33

Table 5.1: Comparison of simulated and observed eigenfrequencies under different temperature scenarios.

Table 5.1 concludes two important features of the data analysis. The first point is related to the response of the FEA results to the scenario-based study. The difference between simulated and observed values for the first mode increases as the temperature decreases, while no consistent trend is evident for the second mode. The FE model captures the change in case of high variable temperature distribution, although on a smaller marginal scale. This signifies that the change in temperature does not imply a change in deformation for the main bridge elements such as steel girders and timber decking, but also a change in the behavior of other components such as the supports or the boundary conditions. The updated model is a deterministic approach that iterates over the same support configuration for all the selected scenarios. This is rooted in the assumption of the FEM where the bridge support does not change their behavior under various temperature conditions. Unlike reality, where the temperature affects the support influence in the bridge vibration (Alampalli, 1998; Cross et al., 2013), the model accounts for the influence of temperature only on the predetermined materials, which include the girders, timber decking governed by the SHELL180 model and the bracings under LINK181 model. The absence of functional models to simulate the supports' behavior under temperature distributions, stems from a dichotomic issue regarding the FEM software limitation, and an epistemic indeterminability of the nature of boundary conditions.

The second feature regards the variation of eigenfrequency between the simulated and observed data. The results of the MAC criterion, shown in Table 5.2, provide a consistency measure for the variation between data. The FE model is significantly less sensitive to temperature changes compared to the observed frequencies. The variation of the MAC values is marginally dependent on the variance of the FEA results, where the variability of the observed eigenfrequencies is the primary driver of the change in MAC values. The first mode shape exhibits a smaller range of variation compared to the second mode with MAC values ranging from 0.967 in the extreme cold scenario to 0.999 in the extreme hot scenario. Given the 0.02% maximal change between FEA results, the change in MAC values is attributed to the more pronounced 7% variation of the observed results. A similar trend applies to the second mode shape, with a bigger variability between the extremely hot afternoon and spring midday MAC values. This variation indicates that the torsional mode shape is more sensitive to the change in temperature distribution compared to the vertical mode shape. A noteworthy result is that of the extremely hot afternoon, which exhibits the highest correlation for the first mode, and the lowest for the second mode, suggesting that the higher average temperature impedes the accuracy of prediction for the higher-order modes.

Scenario	**MAC** f_1	**MAC** f_2
Extreme hot afternoon	0.999	0.885
Cloudy summer afternoon	0.992	0.979
Cloudy autumn afternoon	0.991	0.987
Spring midday	0.979	0.997
Extreme cold sunrise	0.967	0.992

Table 5.2: MAC values under different temperature scenarios.

Despite the relatively high MAC values which are intrinsically related to the average of the results and explicitly to the RMSE values of 0.1621 for the first mode and 0.1723 for the second mode, the findings suggest that the model provides a reasonable approximation of the trends of changing conditions but it can not accurately account for the actual impact of temperature variation on the model compared to the observed data. Thus it requires further investigation of temperature as a time-dependant loading rather than a static force. Other studies of temperature effects on bridge dynamics converge on the same issue (H. Li et al., 2009; Westgate, 2012), where the marginal change in eigenfrequency is explained by the mischaracterization of the subject matter, namely the girders and deck or the input loading relation to stress and strain impact. On the other hand, this explanation does not negate the chance that the observed data are affected by other unconsidered factors in the FE models such as the pedestrians, cyclists, humidity, heat reflection from the pond, etc. that might require a probabilistic account of factors rather than a deterministic approach (Liu and Zhang, 2017).

5.4. Discussion

Understanding the behavior of the infrastructure has prompted engineering knowledge development towards the infrastructure response to variable environmental conditions. This study conducted an exploration of temperature impact on a bridge through the temperature and acceleration analysis obtained from long-term structural health monitoring. The FE model of the bridge was updated to align with the observed frequencies, thereby isolating and investigating the effects of various temperature distributions independently of other factors. The comparison of the two analyses underpins the capability of the FE model in predicting real-life dynamics.

The temperature data included a retrospective examination of historical data, analyzing the temperature distribution in the structures based on a system of thermocouples positioned in two side girders of the bridge. This analysis accounted for diurnal and seasonal complex temperature distributions where the anticipated thermal strain correlated with the position of the sun relative to the bridge, the weather conditions, the average air temperature, etc. Nevertheless, this analysis provided a limited spatial overview of temperature conditioning. The collected data represent a two-dimensional profile of temperature distribution, as the installed thermocouples were fixed at the bottom flange of the girders. Consequently, there was insufficient data to quantify the vertical temperature distribution across the side girder profile or to assess the insulation impact of the timber decking for the solar-isolated middle girder.

Establishing a reference scenario for the study, serving as a baseline for the comparative study was achieved via controlled environment experimentation. Excitation data from heel drops at nine distinct jump locations on the bridge were used to perform a modal analysis. The frequency response function found three principal natural frequencies, with an average of 2.911 Hz, 3.728 Hz, and 8.914 Hz. The respective mode shape was investigated with a phase spectrum analysis. However, the sparse distribution of accelerometers in the bridge impeded the complete modal characterization of the bridge, resulting in low certainty for the mode shapes. The use of a system of wireless sensors, different from the accelerometers of the SHM system implemented in the bridge, underscores the potential discrepancies between the two accelerometers' measurements, particularly concerning the sampling rate and resolution quality.

A numerical replica of the bridge was utilized to analyze the temperature effects on the bridge's dynamic response. The modeling process necessitated several assumptions regarding the geometry and the structural components of the bridge. The real bridge has a slight curvature, unlike the straight geometry simplification modeled in ANSYS. Modeling the slight curvature requires highly refined detailing which would increase the computational power, thereby simplifying the geometrical model was considered feasible since slow curvature has negligible impact on the linear and non-linear analysis compared to the straight model. Furthermore, the connections between timber decking and steel girders are reduced to only the bracings, neglecting the welded steel plates between bracings and girders, timer blocking between girders and timber decking, timber posts and handrails, etc. The inclusion of these details increases model complexity for the sake of negligible impact on the bridge dynamics, thus model geometry optimization guidelines (ANSYS, 2024) provided clear patterns for the simplification of the model. Moreover, the 1/10 meshing ratio employed in Marchenko et al. (2024) was not updated and presumed to be optimal for the modal analysis built upon the static results of the model. Consequently, the sensitivity of the analysis to the discretization size of the model remains to be investigated in future studies.

Before the model is adopted for dynamic analysis, the controlled experimenting results facilitated the updating of the FE model, fitting the model response to real structural behavior. This model updating involved a sensitivity-based approach where the boundary conditions were manually adjusted until a consistent trend of bridge response was evident. Any solution for which the difference between simulated and observed eigenfrequency was below 10% counted for an optimal solution. However, this criterion being empirically based could potentially lead to erroneous results. Despite the sensitivity analysis of the model to stiffness variation, which assisted in a reduction in the error, the reduced stiffness was considered as a uniform 10% reduction for the steel and timber decking, which is an idealized damage quantification. In literature, the damage prominence is delineated from the change in natural frequencies not across the entire structure, but in specific components (Peeters and De Roeck, 2001).

The absence of spatial temperature distribution profiles presented a challenging FE modeling choice. The existing Eurocode guidelines do not adequately address temperature distribution for timber and steel composite bridges, as the commonly used concrete and steel models were unsuitable for the UT Campus bridge. The derivation of the temperature distribution model relied on empirical results from a literature review on steel girders, offering insights into spatial temperature profiles. Nevertheless, a tailor-made distribution for timber decking was not available or modeled and its impact on temperature distribution was not considered.

The study concluded with the comparison of the scenario-based acceleration data and FE simulations. The modal analysis could identify other peaks in Welch's PSD graphs but some limitations arose due to its higher sampling ratio compared to the wireless sensors's sampling rate. The higher sampling rate increases the resolution of frequency distribution, by capturing values that are typically lost during pre-processing steps by filters. Nevertheless, it increases sensitivity to noise which can interfere with the frequency analysis, specifically, the calculation of the normalized PSD values. In some instances, these values were conditioned by some other higher frequency peaks caused by rare event stimuli. Furthermore, the results of this modal analysis are affected by the uncertainty of the response function of the bridge, due to a lack of understanding about the applied force in the structure. The selection criteria to exclude pedestrian movement by considering solely cyclists is insufficient to precisely account for the bridge's natural frequencies. This is explained by the bigger variation of the natural frequencies between scenarios, compared to the FEA simulations. While the FE model proves to capture the trend of the eigenfrequency to decrease as the average temperature increases, it showed to be significantly less sensitive to the temperature change. The model appears to overlook the dynamic impact of temperature while considering it as a static force.

Based on the presented findings, the following recommendations for future studies are made:

1. **Enhanced temperature data collection**: In the case of scenario-based temperature analysis, an updated data collection method is necessary to increase the resolution of temperature distribution. This could require developing a data-driven temperature model capable of extrapolating spatial temperature distribution based on the collected data. Developing the SHM is optional as installing more thermocouples at various profiles would increase the input of the temperature data points.
2. **Scenario-based controlled experimentation**: In the case of controlled experimenting, the same experiment procedure is in different temporal settings or temperature scenarios, rather than relying on a single scenario referencing. This approach would exhaust the need to go through historical data selection, removing the necessity to classify between uncontrolled excitation sources, thereby isolating the temperature effects relative to other variable conditions.
3. **Automatized FE model updating**: The FE model updating process should be systematized and automatized. An extrapolation algorithm of bridge response can be derived from this study to reduce the computational time and effort to find the optimal solution. Implementing a hybrid approach by including Python and Matlab scripting in the APDL environment would be a possible breakthrough for model updating.
4. **Transient thermal analysis**: To further explore the impact of temperature on the structure, a transient analysis incorporating a heat-transfer environment for the FE model could be built using literature support (Westgate (2012), Y. Zhou and Sun (2019), Shan et al. (2023)). This could result in a better approximation of thermal dynamic analysis and a more precise quantification of temperature distribution effects on bridge dynamic parameters.

6

Conclusion

Structural health monitoring of bridges requires high-resolution data to characterize the bridge's dynamic response. The literature highlighted the importance of continuous monitoring to assess the change in bridge response over time. Monitoring environmental conditions alongside bridge response is crucial to account for the real impact of dynamic factors such as temperature variation. Fundamental dynamic properties such as natural frequencies and mode shapes are determining parameters to assess the safety of the bridges as much as quantify the temperature distribution effect in bridges.

This study analyzed field data measured from a structural health monitoring system installed in a bridge, via a temperature analysis of the data from thermocouples and acceleration analysis of data retrieved from the accelerometers. The bridge's fundamental dynamic parameters, including natural frequencies, were determined through a controlled heel-drop experiment on the bridge. To investigate temperature effects on these parameters, numerical replicas of the bridge were adopted in FEM software (ANSYS) by defining the geometrical and material properties. The FE model was updated based on the results of the controlled environment experimentation to match the observed dynamic properties for a given reference scenario. Subsequently, the temperature distributions derived from the temperature analysis of historical data were modeled in ANSYS. The results of the FEA are compared with the scenario-based acceleration data based on statistical and modal error indicators. Based on the results of the implemented methodology in the UT Campus bridge, the following conclusions have been reached:

1. A controlled environment experiment concluded with the approximation of three detected natural frequencies at a temperature of $20\,^{\circ}\mathrm{C}$; the first one is the first symmetrical vertical at 2.911 Hz, the second is the first symmetrical torsional at 3.728 Hz, and the third being the first asymmetrical lateral at 8.914 Hz.
2. The results from the uncontrolled environment are compared to the controlled environment, where the first eigenfrequency changes up to 5% and the second eigenfrequency fluctuates to 1.5%.
3. The model exhibits a high sensitivity to the variation of input parameters, including Young's modulus, with a maximal change of 12% for the first eigenfrequency and 10% for the second eigenfrequency. Sensitivity-based model updating proved to be successful in reducing errors below 10%, with a maximal error of 6% for the second eigenfrequency.
4. The variation in MAC and RMSE values is marginally dependent on the variance of FEA results, with the variability of observed eigenfrequencies being the primary driver of error fluctuation.
5. While the FE model successfully predicts the trend and shows a decrease in eigenfrequency when the average temperature is increasing, it is significantly less sensitive compared to the eigenfrequency variation found in the scenario-based modal analysis.

Structural behavior is a complex phenomenon due to the coupled variability and indeterminacy of the reacting parameters. The precise characterization of bridge parameters including material geometry, density, stiffness, and thermal expansion using deterministic quantification is idealistic thereby serving as an approximate representation of reality. On the other hand, the variable environmental conditions are inherently probabilistic and mechanically intricate to be modeled and quantified precisely. This was reflected by negligible findings in the engineering guidelines about temperature distributions in steel and timber bridges. Furthermore, the thermal characterization of the bridge in ANSYS emphasized the necessity for high-resolution data acquisition, itself inherently dependent on the density of the installed thermocouples. Such a limited spatial overview of temperature distribution led to the addition of a model approximated from the literature review and sparse temperature gradients from the temperature analysis, imposing a linearly dispersed temperature rather than a non-linear temperature distribution. Moreover, accurate quantification of bridge response hinges on our understanding of its dynamic parameters. In scenario-based acceleration analysis, the uncertainty of the bridge response function stems from an incomplete understanding of the input forces. Consequently, scenario selection based on criteria evaluation on the type of input (cyclists, pedestrians, etc) can be insufficient to isolate the bridge's natural response from the resonant frequencies. The comparison of these data with the simulations from ANSYS reveals patterns that highlight the limitations of the FEM. The discrepancy between observed and simulated data suggests the presence of unconsidered factors such as temperature impact on the boundary conditions. Another resolve can be the underestimation of the temperature by considering it as a static force rather than a dynamic one when calculating the stress and strain distributions in the bridge.

The study contributes to the bridge performance evaluation by testing the strengths and limitations of the FEM in predicting bridge behavior under variable temperature conditions. Future studies should focus on enhancing their methodology to address the limitations encountered in this research. Enhancing the data acquisition campaign by data-trained modeling or ML along with high-resolution SHM systems would reduce the encountered uncertainties of the thermal characterization for the bridge. Reducing the uncertainties tied to the scenario-based acceleration data can be exhausted by the implementation of scenario-based controlled experimentation, which would require repetitive controlled experimenting in different temperature conditions. As for the FEM, the model updating can be automatized by the integration of Python or Matlab scripting with the APDL environment to reach an optimal solution. To explore the discrepancies of the prestressed modal analysis, a transient thermal analysis of the bridge, including the heat-transfer modeling could result in a more robust understanding of the temperature distribution effects on bridge dynamic parameters.

References

Alampalli, S. (1998). Influence of in-service environment on modal parameters. *Proceedings-SPIE the international society for optical engineering*, *1*, 111–116.

Alampalli, S. (2000). Effects of testing, analysis, damage, and environment on modal parameters. *Mechanical Systems and Signal Processing*, *14*(1), 63–74. https://doi.org/https://doi.org/10.1006/mssp.1999.1271

ANSYS. (2024). Ansys 10.0 [computer software].

Borah, S., Al-Habaibeh, A., & Kromanis, R. (2021). The effect of temperature variation on bridges—a literature review. *Energy and Sustainable Futures: Proceedings of 2nd ICESF 2020*, 207–212.

Brownjohn, J. M. W., & Xia, P.-Q. (2000). Dynamic assessment of curved cable-stayed bridge by model updating. *Journal of Structural Engineering*, *126*, 252–260.

Cai, J., Qiu, L., Yuan, S., Shi, L., Liu, P., & Liang, D. (2012, August). Structural health monitoring for composite materials. https://doi.org/10.5772/48215

Catbas, F. N., Susoy, M., & Frangopol, D. M. (2008). Structural health monitoring and reliability estimation: Long span truss bridge application with environmental monitoring data. *Engineering Structures*, *30*, 2347–2359. https://doi.org/10.1016/J.ENGSTRUCT.2008.01.013

Cornwell, P., Farrar, C., Doebling, S. W., & Sohn, H. (1999). Environmental variability of modal properties. *Experimental Techniques*, *23*(6), 45–48. https://doi.org/10.1111/j.1747-1567.1999.tb01320.x

Cross, E., Koo, K., Brownjohn, J., & Worden, K. (2013). Long-term monitoring and data analysis of the tamar bridge. *Mechanical Systems and Signal Processing*, *35*(1), 16–34. https://doi.org/https://doi.org/10.1016/j.ymssp.2012.08.026

Eurocode, T. E. U. (2003). Eurocode 1: Actions on structures - part 1-5: General actions - thermal actions [Accessed: 2024-05-31]. https://www.phd.eng.br/wp-content/uploads/2015/12/en.1991.1.5.2003.pdf

Farrar, C. R., Baker, W. E., Bell, T. M., Cone, K. M., Darling, T. W., Duffey, T. A., Eklund, A., & Migliori, A. (1994). *Dynamic characterization and damage detection in the i-40 bridge over the rio grande* (tech. rep. No. LA-12767-MS). Los Alamos National Laboratory.

Figueiredo, E., & Brownjohn, J. (2022). Three decades of statistical pattern recognition paradigm for shm of bridges. *Structural Health Monitoring*, *21*(6), 3018–3054. https://doi.org/10.1177/14759217221075241

Figueiredo, E., Peres, N., Moldovan, I., & Nasr, A. (2024). Impact of climate change on long-term damage detection for structural health monitoring of bridges. *Structural Health Monitoring*. https://doi.org/10.1177/14759217231224254

Glashier, T., Kromanis, R., & Buchanan, C. (2024). Temperature-based measurement interpretation of the mx3d bridge. *Engineering Structures*, *305*, 116736. https://doi.org/https://doi.org/10.1016/j.engstruct.2023.116736

Guo, F., Zhang, S., Duan, S., Shen, Z., Yu, Z., Jiang, L., & He, C. (2023). Temperature gradient zoning of steel beams without paving layers in china. *Case Studies in Construction Materials*, *18*, e02054. https://doi.org/10.1016/j.cscm.2023.e02054

Kangas, S., Wang, X., Padur, D., Li, Z., Lui, L., Helmicki, A., & Hunt, V. (2003). Field test-based calibration of bridge finite element models for condition assessment. *Proceedings of ASNT Structural Materials Technology VI: An NDT Conference*.

Koo, K., Brownjohn, J., List, D., & Cole, R. (2012). Structural health monitoring of the tamar suspension bridge. *Structural Control & Health Monitoring*, *20*(4), 609–625. https://doi.org/10.1002/stc.1481

Kromanis, R., Kripakaran, P., & Harvey, B. (2015). Long-term structural health monitoring of the cleddau bridge: Evaluation of quasi-static temperature effects on bearing movements. *Structure and Infrastructure Engineering*, 1342–1355. https://doi.org/10.1080/15732479.2015.1117113

Kromanis, R. (2021). Characterizing footbridge response from cyclist crossings with computer vision-based monitoring. *International Workshop on Civil Structural Health Monitoring*, 83–95.

Laory, I., Hadj Ali, N. B., Trinh, T. N., & Smith, I. F. (2012). Measurement system configuration for damage identification of continuously monitored structures. *Journal of Bridge Engineering*, *17*(6), 857–866.

Li, H., Li, S., Ou, J., & Li, H. (2009). Modal identification of bridges under varying environmental conditions: Temperature and wind effects [Advance online publication. doi:10.1002/stc.319]. *Structural Control & Health Monitoring*.

Li, S., Li, H., Liu, Y., Lan, C., Zhou, W., & Ou, J. (2014). Smc structural health monitoring benchmark problem using monitored data from an actual cable-stayed bridge. *Structural Control and Health Monitoring*, *21*, 156–172.

Liu, Y., & Zhang, S. (2017). Probabilistic baseline of finite element model of bridges under environmental temperature changes. *Computer-aided Civil and Infrastructure Engineering*, *32*(7), 581–598. https://doi.org/10.1111/mice.12268

Malekloo, A., Ozer, E., AlHamaydeh, M., & Girolami, M. (2021). Machine learning and structural health monitoring overview with emerging technology and high-dimensional data source highlights. *Structural Health Monitoring*.

Mao, Q., Mazzotti, M., DeVitis, J., Braley, J., Young, C., Sjoblom, K., & Bartoli, I. (2019). Structural condition assessment of a bridge pier: A case study using experimental modal analysis and finite element model updating. *Structural Control and Health Monitoring*, *26*(1), e2273.

Marchenko, A., Kromanis, R., & Dorée, A. G. (2024). Characterizing bridge thermal response for bridge load rating and condition assessment: A parametric study. *Infrastructures*, *9*(2), 20.

Mariani, S., Kalantari, A., Kromanis, R., & Marzani, A. (2024). Data-driven modeling of long temperature time-series to capture the thermal behavior of bridges for shm purposes. *Mechanical Systems and Signal Processing*, *206*, 110934. https://doi.org/10.1016/j.ymssp.2024.110934

Moorty, S., & Roeder, C. W. (1992). Temperature□dependent bridge movements. *Journal of Structural Engineering*, *118*(4), 1090–1105. https://doi.org/10.1061/(ASCE)0733-9445(1992)118:4(1090)

Ni, Y., Zhou, H. F., Chan, K., & Ko, J. M. (2008). Modal flexibility analysis of cable□stayed ting kau bridge for damage identification. *Computer-Aided Civil and Infrastructure Engineering*, *23*(3), 223–236. https://doi.org/10.1111/j.1467-8667.2008.00521.x

Peeters, B., & De Roeck, G. (2000). One year monitoring of the z24 bridge: Environmental influences versus damage effects. *Proc. IMAC-XVIII*, 1570–1576.

Peeters, B., & De Roeck, G. (2001). One-year monitoring of the z24-bridge: Environmental effects versus damage events. *Earthquake Engineering & Structural Dynamics*, *30*(2), 149–171. https://doi.org/https://doi.org/10.1002/1096-9845(200102)30:2<149::AID-EQE1>3.0.CO;2-Z

Poudel, A., Kim, S., Cho, B. H., & Kim, J. (2024). Temperature effects on the natural frequencies of composite girders. *Applied Sciences*, *14*(3), 1175. https://doi.org/10.3390/app14031175

Rao, S. S. (2017). *The finite element method in engineering*. Butterworth-Heinemann.

Ren, W., Zhao, T., & Harik, I. (2004). Experimental and analytical modal analysis of steel arch bridge. *Journal of Structural Engineering*, *130*(7), 1022–1031.

Rijkswaterstaat. (2022, July). *Impact analyses for bridges and viaducts* (tech. rep.) (Final evaluation report on bridges and viaducts; Impact Analyses; Probabilistic analyses for determining the impact on the structural safety of bridges and viaducts).

Rishin, V. V., Lyashenko, B. A., Akinin, K. G., & Nadezhdin, G. N. (1973). Temperature dependence of adhesion strength and elasticity of some heat-resistant coatings. *Strength of Materials*, *5*(1), 123–126. https://doi.org/10.1007/bf00762888

Rogers, M. J., Hrovat, K., McPherson, K., Moskowitz, M. E., & Reckart, T. (1997). *Accelerometer data analysis and presentation techniques* (tech. rep. No. NAS 1.15: 113173).

Shan, Y., Li, L., Xia, Q., Gao, W., Jing, Q., & Xia, Y. (2023). Temperature behavior of cable-stayed bridges. part i — global 3d temperature distribution by integrating heat-transfer analysis and field monitoring data. *Advances in Structural Engineering*, *26*(9), 1579–1599. https://doi.org/10.1177/13694332231174258

Sohn, H. (2006). Effects of environmental and operational variability on structural health monitoring. *Philosophical Transactions of the Royal Society A*, *365*(1851), 539–560. https://doi.org/10.1098/rsta.2006.1935

Steenackers, G., & Guillaume, P. (2005). Structural health monitoring of the z24 bridge in presence of environmental changes using modal analysis. *Proceedings of IMAC*, *23*.

Tadeu, A., Romero, A., Bandeira, F., Pedro, F., Dias, S., Serra, M., & Galvin, P. (2022). Theoretical and experimental analysis of the quasi-static and dynamic behaviour of the world's longest suspension footbridge in 2020 [Advance online publication]. *Engineering Structures*, *253*. https://doi.org/10.1016/j.engstruct.2021.113830

Wang, Y., Zhan, Y., Zhao, R., & Author(s), T. (2016). Analysis of thermal behavior on concrete box-girder arch bridges under convection and solar radiation. *Advances in Structural Engineering*, 1043–1059. https://doi.org/10.1177/1369433216630829

Westgate, R. (2012). *Environmental effects on a suspension bridge's performance* [Doctoral dissertation]. University of Sheffield.

Westgate, R., & Brownjohn, J. (2011). Development of a tamar bridge finite element model. *Conference proceedings of the Society for Experimental Mechanics*, 13–20. https://doi.org/10.1007/978-1-4419-9825-5_2

Xia, Y., Hao, H., Zanardo, G., & Deeks, A. (2006). Long term vibration monitoring of an rc slab: Temperature and humidity effect. *Engineering Structures*, *28*(3), 441–452. https://doi.org/https://doi.org/10.1016/j.engstruct.2005.09.001

Zhou, L., Xia, Y., Brownjohn, J., & Koo, K. Y. (2015). Temperature analysis of a long-span suspension bridge based on field monitoring and numerical simulation. *Journal of Bridge Engineering*, *21*, 04015027. https://doi.org/10.1061/(ASCE)BE.1943-5592.0000786

Zhou, Y., & Sun, L. (2019). A comprehensive study of the thermal response of a long-span cable-stayed bridge: From monitoring phenomena to underlying mechanisms. *Mechanical Systems and Signal Processing*, *124*, 330–348. https://doi.org/10.1016/j.ymssp.2019.01.045

Zhu, Q., Xu, Y., & Xiao, X. (2015). Multiscale modeling and model updating of a cable-stayed bridge. i: Modeling and influence line analysis. *Journal of Bridge Engineering*, *20*, 04014112.

A

Appendices

A.1. Temperature distribution in ANSYS

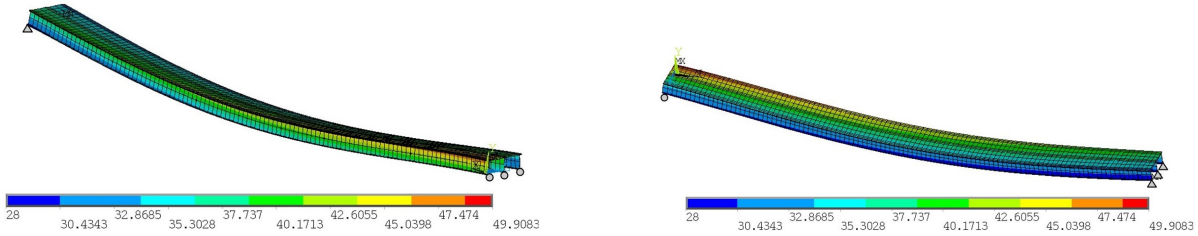

(a) **(b)**

Figure A.1: Temperature distribution for an extremely hot afternoon from (a) southwest and (b) northeast.

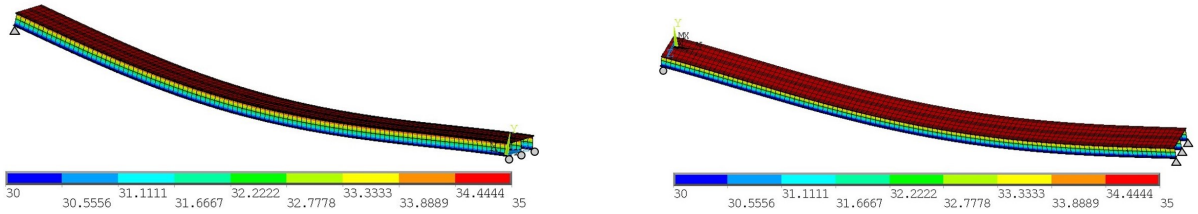

(a) **(b)**

Figure A.2: Temperature distribution for a cloudy summer afternoon from (a) southwest and (b) northeast.

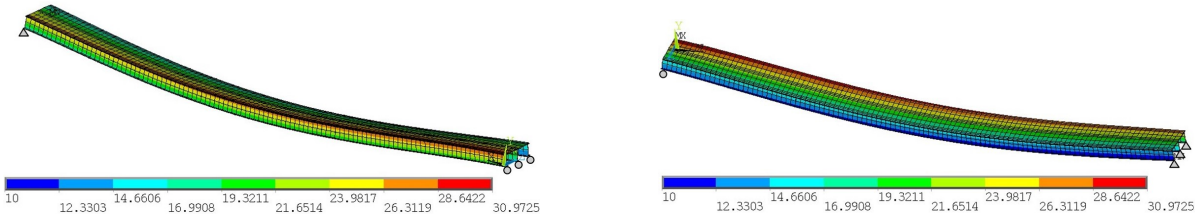

(a) **(b)**

Figure A.3: Temperature distribution for a spring midday from (a) southwest and (b) northeast.

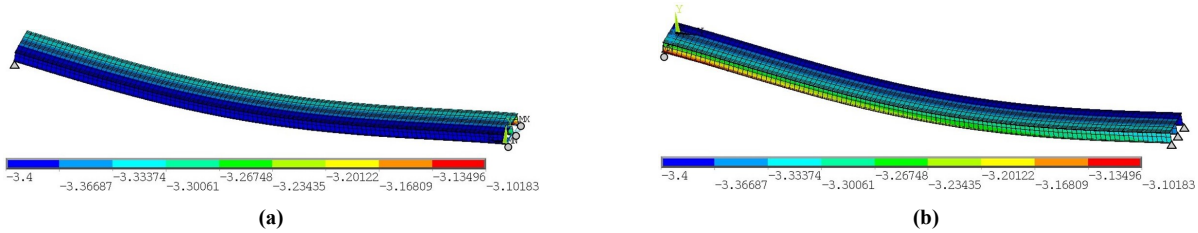

(a) **(b)**

Figure A.4: Temperature distribution for an extremely cold sunrise from (a) southwest and (b) northeast.

A.2. Experimental-based mode shapes

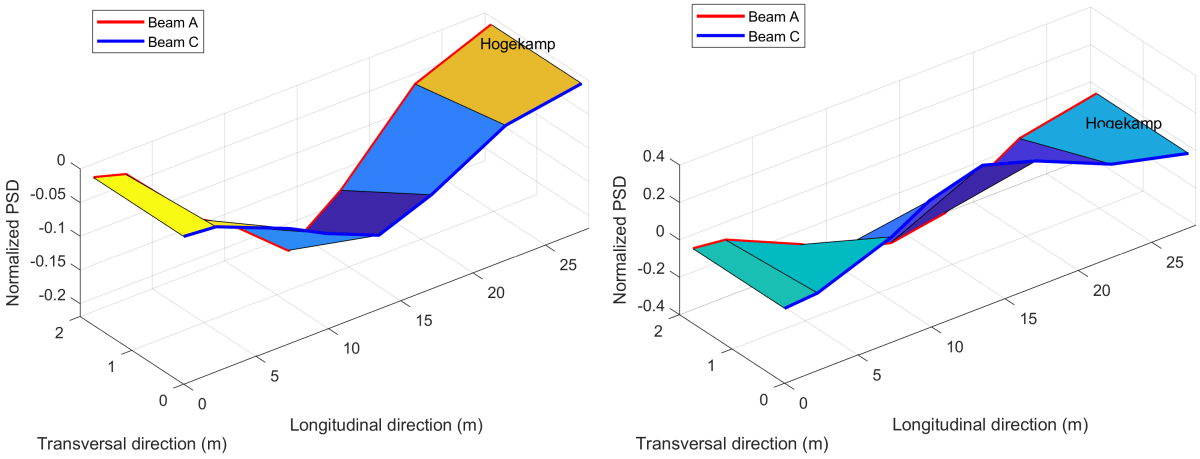

(a) VS1 = 2.955 Hz **(b)** TS1 = 3.709 Hz

Figure A.5: Scenario-based results of the extremely hot afternoon for (a) first symmetrical vertical and (b) first symmetrical torsional mode shape.

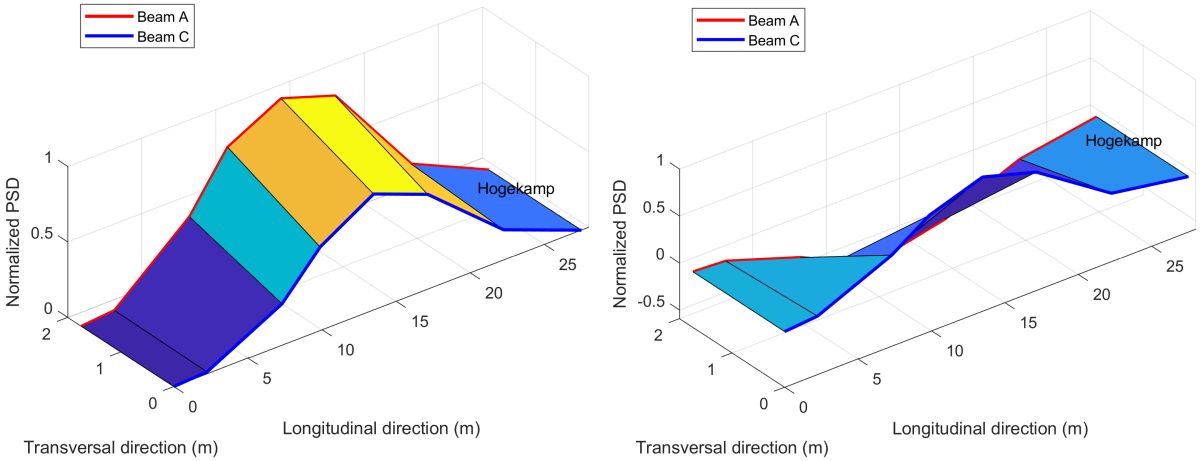

(a) VS1 = 3.021 Hz **(b)** TS1 = 3.723 Hz

Figure A.6: Scenario-based results of the cloudy summer afternoon for (a) first symmetrical vertical and (b) first symmetrical torsional mode shape.

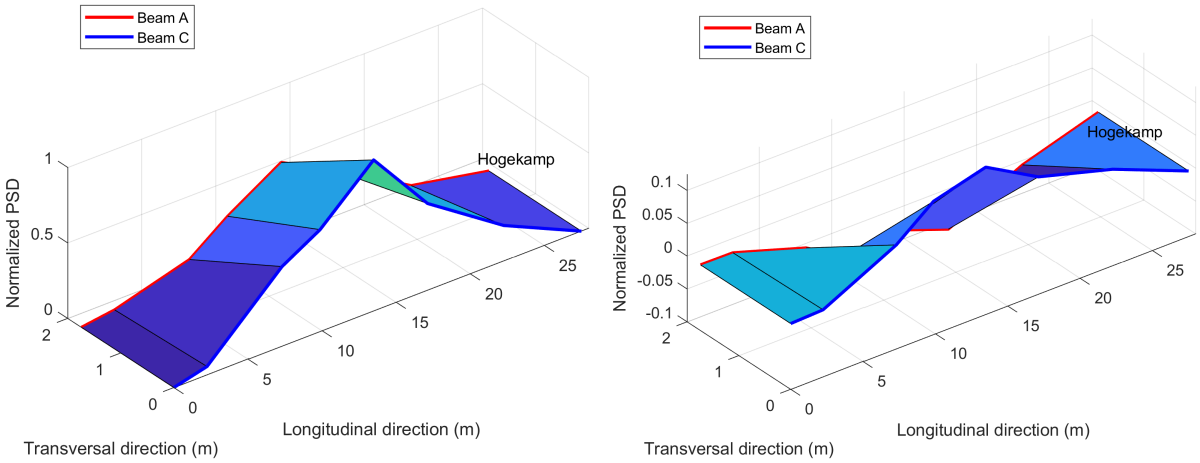

(a) VS1 = 3.143 Hz **(b)** TS1 = 3.938 Hz

Figure A.7: Scenario-based results of the spring midday for (a) first symmetrical vertical and (b) first symmetrical torsional mode shape.

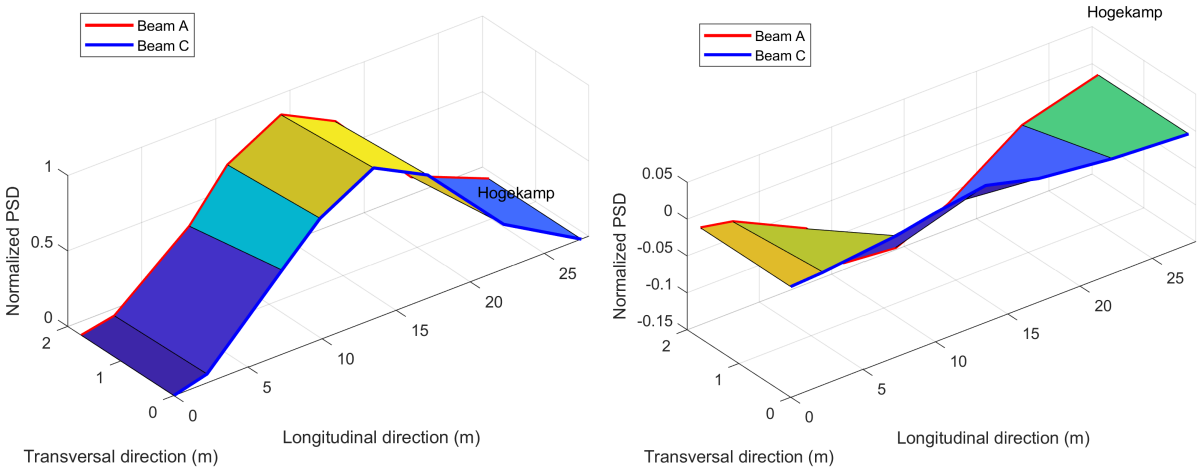

(a) VS1 = 3.178 Hz **(b)** TS1 = 3.906 Hz

Figure A.8: Scenario-based results of the extremely cold sunrise for (a) first symmetrical vertical and (b) first symmetrical torsional mode shape.

A.3. Simulated mode shapes

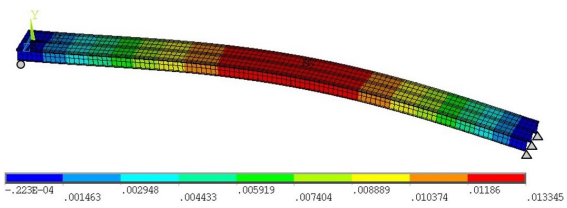

(a) VS1 = 2.929 Hz

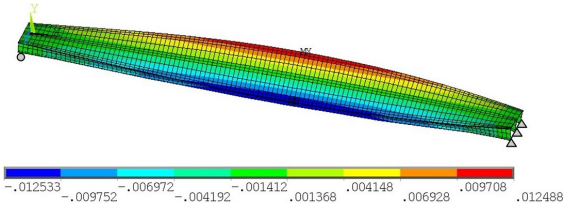

(b) TS1 = 3.956 Hz

Figure A.9: FEA results of the extreme hot afternoon for (a) first symmetrical vertical, and (b) first symmetrical torsional mode shape.

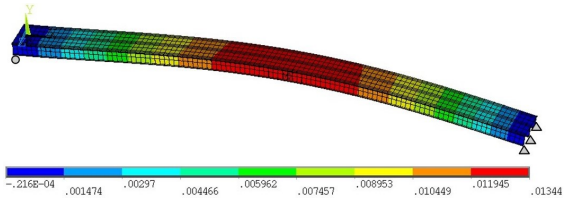

(a) VS1 = 2.929 Hz

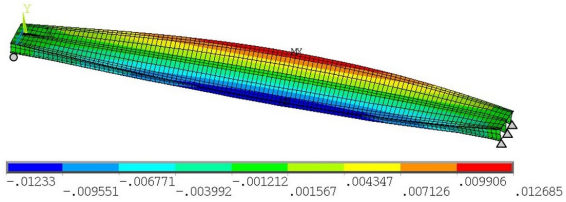

(b) TS1 = 3.956 Hz

Figure A.10: FEA results of the cloudy summer afternoon for (a) first symmetrical vertical, and (b) first symmetrical torsional mode shape.

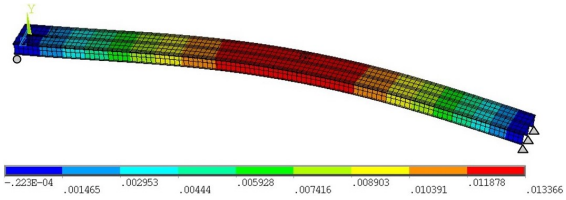

(a) VS1 = 2.9296 Hz

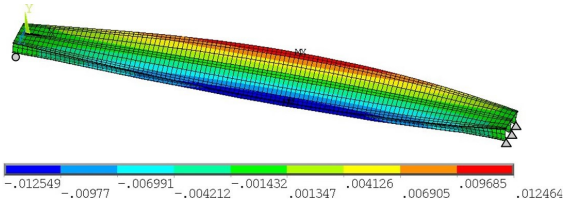

(b) TS1 = 3.959 Hz

Figure A.11: FEA results of the spring midday for (a) first symmetrical vertical, and (b) first symmetrical torsional mode shape.

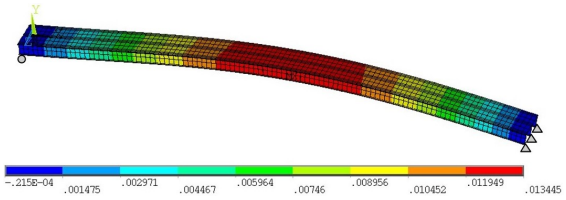

(a) VS1 = 2.9298 Hz

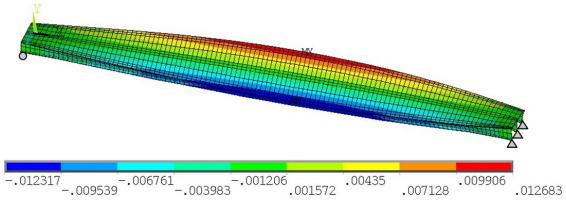

(b) TS1 = 3.958 Hz

Figure A.12: FEA results of the extreme cold sunrise for (a) first symmetrical vertical, and (b) first symmetrical torsional mode shape.